Biochemical Journal (2020) **477** 3673–3693
https://doi.org/10.1042/BCJ20200240

Research Article

Three cytosolic NAD-malate dehydrogenase isoforms of *Arabidopsis thaliana*: on the crossroad between energy fluxes and redox signaling

Aleksandra Liszka[1,*†], Regina Schimpf[1,*], Krupskaya Ivannova Cartuche Zaruma[1,*], Annika Buhr[1], Thorsten Seidel[2,3], Stefan Walter[4], Johannes Knuesting[1], Anna Dreyer[3], Karl-Josef Dietz[3], Renate Scheibe[1] and Jennifer Selinski[1,3,5‡]

[1]Department of Plant Physiology, Faculty of Biology/Chemistry, Osnabrueck University, Osnabrueck, Germany; [2]Dynamic Cell Imaging, Faculty of Biology, Bielefeld University, Bielefeld, Germany; [3]Department of Biochemistry and Physiology of Plants, Faculty of Biology, Bielefeld University, Bielefeld, Germany; [4]Mass-Spectrometry Unit, Faculty of Biology/Chemistry, Osnabrueck University, Osnabrueck, Germany; [5]Department of Animal, Plant, and Soil Science, Australian Research Council Centre of Excellence in Plant Energy Biology, School of Life Science, La Trobe University Bundoora, Bundoora, Australia

Correspondence: Jennifer Selinski (jennifer.selinski@uni-bielefeld.de)

In yeast and animal cells, mitochondrial disturbances resulting from imbalances in the respiratory chain require malate dehydrogenase (MDH) activities for re-directing fluxes of reducing equivalents. In plants, in addition to mitochondria, plastids use malate valves to counterbalance and maintain redox-homeostasis. Arabidopsis expresses three cytosolic MDH isoforms, namely cyMDH1, cyMDH2, and cyMDH3, the latter possessing an N-terminal extension carrying a unique cysteine residue C2. In this study, redox-effects on activity and structure of all three cyMDH isoforms were analyzed *in vitro*. cyMDH1 and cyMDH2 were reversibly inactivated by diamide treatment, accompanied by dimerization via disulfide-bridge formation. In contrast, cyMDH3 forms dimers and higher oligomers upon oxidation, but its low specific activity is redox-independent. In the presence of glutathione, cyMDH1 and cyMDH2 are protected from dimerization and inactivation. In contrast, cyMDH3 still dimerizes but does not form oligomers any longer. From analyses of single and double cysteine mutants and structural modeling of cyMDH3, we conclude that the presence of C2 and C336 allows for multiple cross-links in the higher molecular mass complexes comprising disulfides within the dimer as well as between monomers of two different dimers. Furthermore, nuclear localization of cyMDH isoforms was significantly increased under oxidizing conditions in isolated Arabidopsis protoplasts, in particular of isoform cyMDH3. The unique cyMDH3 C2–C2-linked dimer is, therefore, a good candidate as a redox-sensor taking over moonlighting functions upon disturbances of energy metabolism, as shown previously for the glycolytic enzyme glyceraldehyde 3-phosphate dehydrogenase (GAPDH) where oxidative modification of the sensitive catalytic cysteine residues induces nuclear translocation.

*These authors contributed equally to this work.
†Present address: Department of Plant Biotechnology, Faculty of Biochemistry, Biophysics and Biotechnology, Jagiellonian University, Gronostajowa 7, Krakow 30-387, Poland
‡Present address: Department of Biochemistry and Physiology of Plants, Faculty of Biology, Bielefeld University, Bielefeld, Germany

Received: 23 March 2020
Revised: 4 September 2020
Accepted: 7 September 2020

Accepted Manuscript online: 8 September 2020
Version of Record published: 5 October 2020

Introduction

Malate dehydrogenases (MDHs) are essential components of shuttle systems enabling the indirect transfer of reducing equivalents received from NAD(H) or NADP(H) between subcellular compartments in all eukaryotic cells. MDHs are widely distributed oxidoreductases catalyzing the reversible interconversion of malate and oxaloacetate (OAA). These dicarboxylic acids are exchanged between cell compartments by specific translocators and are required for the distribution of reducing equivalents across cellular membranes. Systems consisting of MDHs and malate/OAA translocators are described as malate valves enabling indirect transport of reducing equivalents [1,2]. MDH isoforms occur in the cytosol, mitochondria, peroxisomes as well as in plastids. Both mitochondria and chloroplasts with their electron

Biochemical Journal (2020) 477 3673–3693
https://doi.org/10.1042/BCJ20200240

transport chains carry the risk of excessive reactive oxygen species (ROS) formation upon redox-imbalances. To counteract oxidative damage, fluxes of reducing equivalents are controlled by MDH isoforms in the respective compartment to maintain redox-homeostasis. While most MDH isoforms are NAD-dependent, chloroplasts additionally possess a unique NADP-dependent isoform that is post-translationally regulated by redox mechanisms. Its N- and C-terminal extensions, each carrying two regulatory cysteine residues, are reversibly oxidized by disulfide-bridge formation. We and others have previously characterized this redox regulatory mechanism allowing for switching activity on in the light, and off within seconds when photosynthetic electron transport stops upon darkening [3,4]. Furthermore, the adjustment of actual activities and fluxes is tightly controlled with the help of small molecules affecting the rates of reduction and oxidation. For instance, $NADP^+$ acts negatively on the reductive activation of NADP–MDH [5–7]. All eukaryotic organisms rely on the adjustment of central metabolism for controlled energy supply, in particular in response to changing (environmental) conditions. These processes are most challenging and complex in sessile plants.

Recently, metabolic enzymes such as MDHs came into the focus of research attempts to identify specific targets in energy metabolism for cancer therapy [8,9]. Cytosolic glyceraldehyde 3-phosphate dehydrogenase (GAPDH) involved in glycolysis, but also MDH, participates in adjusting energy supply in proliferating cancer cells and during induction of autophagy [10–12]. Strict cooperation between cytosolic MDH and glycolysis likely supports the high glycolytic rates in proliferating cells [13]. Cytosolic MDHs play important roles in various cancer types, such as lung carcinoma [14,15] and pancreatic ductal adenocarcinoma [11]. They participate in cell-specific activities during development [16], osteoclastogenesis [17], and senescence [18].

The fundamental importance of oxidoreductases in energy metabolism together with the occurrence of various enzymes of central metabolism in the nucleus gave rise to the active research field aiming to understand the moonlighting functions of these enzymes that undergo some direct post-translational modification before they take over new tasks [19]. For instance, nuclear translocation of GAPDH and MDH were shown to induce the transcription of enzymes required for coping with cadmium stress in the yeast *Candida tropicalis* [20]. Connected with multiple pathological disorders, disturbance of the cellular redox-homeostasis is now accepted as the central event that should be counterbalanced by proper therapies [21].

As previously shown for cytosolic GAPDH, changed properties of the oxidized forms of MDHs are hypothesized to activate moonlighting functions that link energy metabolism to adaptive responses required for maintenance of redox-homeostasis [22,23]. Redox-dependent reversible inactivation and covalent dimerization have also been shown to occur when Arabidopsis cyMDH1 is subjected to oxidation [24,25]. This work aimed to scrutinize the redox-properties of the three cyMDH isoforms from *A. thaliana* in order to provide evidence for sensing and signaling roles of cyMDHs in the nucleus.

Experimental procedures

Isolation of Arabidopsis mesophyll protoplasts and localization of cyMDH isoforms

The cDNA encoding the open reading frame of cyMDH1, cyMDH2, and cyMDH3 (for primers see Supplementary Table S1) was cloned into the vector pGFP2 (restriction sites: XbaI/XhoI) to generate cyMDH1–, cyMDH2–, and cyMDH3–GFP gene fusions driven by the CaMV-35S promoter as described by [26]. The protoplast isolation and transfection were performed as described before by [27]. The co-localization was analyzed by confocal laser scanning microscopy (LSM780, Zeiss) using a water immersion objective with 63-fold magnification (Zeiss LCI Plan-Neofluar 63×/1.3 Immersion Korr DIC M27). GFP and mCherry were excited sequentially by the 488 nm line of an argon-ion laser and the 561 nm line of a DPSS laser, respectively. The choice of laser lines required the main beam splitter MBS488/561. Emission was recorded in three channels: GFP between 500 and 550 nm (shown in green), mCherry between 571 and 651 nm (shown in magenta), and chlorophyll between 651 and 700 nm (shown in blue). The pinhole was set to Airy 1–3 corresponding to a diameter of 63–166 μm, the pixel dwell time was in the range of 10 to 16 μs due to a line averaging of four. 12-bit encoded fluorescence images were analyzed with the co-localization analysis tool of the ZEN black edition software: Co-localization was quantified by plotting the intensities in the GFP channel against the intensities in the mCherry channel followed by correlation analysis. The degree of co-localization between cyMDH–GFP fusions and bZIP-mCherry is given as correlation coefficient R and describes the nuclear localization of the cyMDH isoforms. Cells were treated for 2 h with 0.5% DMSO (mock treatment) or 2.5 mM diamide

(diazenedicarboxylic acid bis[N,N-dimethylamide]), for 1 h with 20 mM DTT, 200 μM H_2O_2, 50 μM S-nitroso glutathione (GSNO), or 100 μM sodium nitroprusside (SNP). Untreated cells served as a control.

Cloning and purification of cyMDH isoforms and their cysteine mutants

A. thaliana ecotype Columbia (Col-0) plants were cultivated for 6 weeks in a growth chamber on soil under short-day conditions with 7.5 h light and a light intensity of 150 μE m^{-2} s^{-1} at 20°C. Total RNA was isolated from 100 mg frozen leaf material using TRI Reagent (Molecular Research Center, Cincinnati, U.S.A.) as described in the protocol of the supplier. From 5 μg total RNA, cDNA was synthesized using oligo (dT) as primers provided with the kit, according to the instructions of the supplier (ThermoFisher Scientific, Darmstadt, Germany; RevertAid™ First Strand cDNA Synthesis Kit).

cyMDH1, cyMDH2, and cyMDH3 were amplified with the primers cyMDH1_for/cyMDH1_rev, cyMDH2_for/cyMDH2_rev, and cyMDH3_for/cyMDH3_rev (Supplementary Table S1) containing BamHI, NdeI or XhoI restriction sites for cloning. After PCR amplification, the cyMDH fragments were ligated into sticky-end restricted vector pGEM-T Easy according to the instructions of the supplier (pGEM®-T Easy Vector Systems, Promega). After restriction with NdeI/BamHI (cyMDH1), NdeI/XhoI (cyMDH2) or XhoI/BamHI (cyMDH3), the 1011-bp (cyMDH1), 1015-bp (cyMDH2), and 1019-bp (cyMDH3) fragments were introduced into the correspondingly restricted expression vector pET-16b (Novagen; Merck Chemicals, Darmstadt, Germany).

Cysteine residues of cyMDH1, cyMDH2, and cyMDH3 were substituted via site-directed mutagenesis according to the instructions of the supplier (Q5® Site Directed Mutagenesis Kit, New England Biolabs). For PCR amplification, the PfuUltra II Fusion HS DNA-Polymerase (Agilent Technologies, Santa Clara, U.S.A.) and the specific mutagenesis primers (Supplementary Table S1) were used. Following PCR, products were treated for 1 h at 37°C with DpnI, which specifically digests methylated DNA to eliminate the maternal DNA template. The PCR-derived constructs were verified by DNA sequencing through the ligation sites.

The *E. coli* mutant strain BL21 (DE3) pLysS was transformed with the respective constructs. A 5 ml overnight culture was used to inoculate 600 ml YT medium containing 100 μg/ml ampicillin. Cells were cultivated at 37°C under shaking at 160 rpm. After reaching an OD_{600} of 0.4–0.6, the protein expression was induced by the addition of 1 mM isopropyl-β-D-thiogalactopyranoside. The cells were incubated at 15°C and 200 rpm for further 12 h and were harvested by centrifugation (5000×***g***, 20 min, 4°C). The pellet was frozen in liquid nitrogen and stored at −80°C. For protein purification, the cells were thawed, resuspended in washing buffer (50 mM Tris–HCl, pH 7.5, 150 mM NaCl, 5 mM imidazole) and disrupted by ultrasonication (Vibracell, Fisher Scientific, Illkirch, France). After centrifugation (10 000×***g***, 30 min, 4°C) the supernatant was incubated with Ni-Sepharose 6 Fast Flow (GE Healthcare, Munich, Germany) for 30 min at 4°C in a tube rotary shaker. After exhaustive washing, the N-terminal His-tagged protein was eluted with elution buffer (50 mM Tris–HCl, pH 7.5, 150 mM NaCl, 250 mM imidazole). For size-exclusion chromatography, the samples were reduced (5 mM DTT) and loaded onto a pre-equilibrated column (Merck, Darmstadt, Germany) connected to an ÄKTAprime plus chromatography system (GE Healthcare). After checking by SDS–PAGE, only highly pure fractions were concentrated and stored at −20°C in the final buffer (50 mM Tris–HCl, pH 7.5, 150 mM NaCl; 10% (v/v) glycerol).

Mass-spectrometric analysis of Cys-containing tryptic peptides

The individual gel slices were washed and treated with 100 mM iodoacetamide. The digestion was started by adding trypsin (Promega V5511) and samples were incubated for 16 h at 37°C. Subsequently, the peptide-containing supernatant was centrifuged to remove any particles and transferred in HPLC vials. All following chromatographically steps were carried out with an Ultimate 3000 Nano HPLC (ThermoFisher): The first 10 μl of samples were desalted and concentrated using a precolumn (ThermoFisher, C18 PepMap 5 μm, 100 Å with a dimension of 300 μm (inner diameter) × 5 mm length). The corresponding solvent was water supplemented with 0.1% trifluoroacetic acid at a flow rate of 25 μl/min.

The loaded and washed precolumn was switched into the 'nano flow line' (250 nl/min), where an Easy Spray column (ThermoFisher, PepMap RSLC C18, 2 μm 100 Å with dimension of 75 μm (inner diameter) and 500 mm (length) was mounted at the end. Peptides were eluted by changing the buffer A (water, 0.1% formic acid) to 80% of buffer B (80% acetonitrile, 20% water and 0.1% formic acid) continuously in 160 min. The electro-spray ionization (ESI) was done at 1500 V (ESI Spray Source, ThermoFisher).

A Q-Exactive-Plus orbitrap mass spectrometer (ThermoFisher) was used to determine the MS as well as the MSMS (HCD fragmentation) data under the conditions described in Supplementary Table S4.

Biochemical Journal (2020) 477 3673–3693
https://doi.org/10.1042/BCJ20200240

The collected data were subsequently loaded into Peaks Studio X (Bioinformatics Solution Inc., Canada). The peptides were identified using a DeNovo approach and the corresponding proteins by a DB-search. The database contained the individual trypsin peptides of the corresponding cyMDH sequence as well as all concatenates of cysteine-containing peptides in different arrangement. For both searches (DeNovo and DB) the MS tolerance was adjusted to 15 ppm, the MSMS tolerance to 0.2 Da. As variable post-translational modifications carbamidomethylation of cysteines (+58 Da), S-glutathionlylation of cysteines (+305 Da) and half of a disulfide bridge (+8 Da = +1/2 H_2O–1H) were chosen.

Determination of NAD–MDH activity

The different cyMDH samples (1 μg/μl) were pre-reduced in the presence of 0.5 mM DTT for 30 min at room temperature in exchange buffer (35 mM Tris–HCl, pH 8.8). Before the oxidative treatment was started, enzyme activities of reduced cyMDHs were recorded. To determine the cyMDH activity, proteins were diluted to a final concentration of 2 ng/μl in reaction buffer (0.1 M Tris–HCl, pH 8.0, bovine serum albumin (0.1 mg/ml), 10 mM $MgCl_2$, 0.2 mM NADH). Cuvettes were filled with 985 μl of reaction buffer and 5 μl sample containing 10 ng protein. After baseline determination, the substrate oxaloacetate (OAA) (1 mM) was added and the cyMDH activity recorded at 334 nm for 5 min using a spectrophotometer (SPECORD 50, Analytik Jena). After activity determination of the fully reduced enzyme, the DTT-containing samples were desalted (Desalting Spin Columns, Thermo Scientific). After the removal of DTT, the proteins were oxidized by incubation with 0.5 mM diamide for 30 min. To estimate the protective properties of small molecules on cyMDH oxidation, GSH, NAD^+, NADH, $NADP^+$, NADPH, OAA, or malate, at the given concentrations, were added before the oxidative treatment. After determining the activity of the oxidatively treated cyMDHs, 20 mM DTT was used to check the reversibility of the oxidation process. Data are means from three independent experiments with three technical replicates each.

Non-reducing gel electrophoresis

For the non-reducing SDS–PAGE, pre-cast Tris-glycine NB 12% gels (NuSep, Germantown U.S.A.) were used. The protein samples (5 μg) were first pre-reduced for 30 min at room temperature using 5 mM DTT. After desalting, the samples were oxidized for 30 min in the presence of 5 mM diamide. As controls, samples were re-reduced with 20 mM DTT for 30 min. Free thiol groups were blocked with 30 mM iodoacetamide. The samples were incubated in loading dye without DTT at 95°C for 5 min. The Page Ruler Prestained Protein Ladder (Thermo Scientific) served as molecular mass standard. The electrophoresis was carried out at a constant voltage of 120 V for ∼1 h. For staining, the gel was incubated overnight in a Coomassie solution and then destained. For the documentation, the gel was photographed using the GelDoc system (Bio-Rad, Feldkirchen, Germany).

Non-reducing native PAGE was performed as described in [28]. Samples were separated on a 12% (w/v) gel. The NativeMark Unstained Protein Standard (Invitrogen) served as molecular mass standard. All electrophoretic separations were performed in a cold room at 4°C at a constant current of 60 mA for 1 h. Gels were stained with Coomassie brilliant blue R-250.

Structural modeling

The *A. thaliana* cyMDH1, cyMDH2, and cyMDH3 amino acid sequences were obtained from the Arabidopsis Information Resource (TAIR). While the structure of cyMDH1 was previously resolved by [25], structural models of cyMDH2 and cyMDH3 are lacking so far. Therefore, the sequences of cyMDH2 and cyMDH3 were used to calculate the corresponding structures via raptorX [29]. These structures were used to generate dimeric models of cyMDH2 and cyMDH3 using the GalaxyHomomer web server [30]. The top-scoring structures together with the resolved structure of cyMDH1 (pdb: 5nuf) were then used to analyze the structural models of cyMDH1, cyMDH2, and cyMDH3 using Pymol version 2.1 [31] together with the ABPS/pdb2pqr plugin [32–34].

Results

Expression pattern of cyMDH isoforms

In *A. thaliana*, nine genes encode MDH isoproteins, three of them representing cytosolic NAD-dependent malate dehydrogenases (cyMDH). The expression of cyMDH genes is almost constitutive throughout plant development but to a varying extent: cyMDH1 (At1g04410) represents the major isoform exhibiting the

highest transcript abundance, cyMDH2 (At5g43330) transcript amounts are lower, and cyMDH3 (At5g56720) is the least represented isoform (Supplementary Figure S1). The cytosolic isoforms do not possess transit peptides in contrast with the organellar isoforms, namely the NAD-dependent MDH in plastids (At3g47520), the two in mitochondria (At3g15020, At1g53240), and the other two in peroxisomes (At2g22780, At5g09660). From phylogenetic analyses of Arabidopsis MDH proteins, a close relationship of cyMDHs with the chloroplast NADP–MDH (At5g58330; 41% identity, regulatory extensions excluded) had been found [35]. Among the three cytosolic isoforms, six cysteine residues are highly conserved (C79, C125, C155, C252, C292, and C330 in cyMDH1 and cyMDH2). However, cyMDH3 is unique possessing two additional cysteine residues: A unique one in the N-terminal extension carrying a cysteine residue at position 2 (C2) and another one near the C-terminus (C279) (Figure 1).

Enzyme activities of recombinant cyMDH isoforms

First, the effect of oxidation on the specific activities of cyMDH isoforms was analyzed. Although the recombinant enzymes were active after purification with Ni^{2+}-chelating chromatography, they were routinely pre-incubated with 0.5 mM DTT (pH 8.8) to convert them into the fully reduced form and to remove any pre-existing cysteine modifications. When assayed in the direction of malate formation, cyMDH1 and cyMDH2 exhibit specific activities of ∼2000 U/mg protein, while cyMDH3 is characterized by a significantly lower V_{max} of ∼500 U/mg protein (Figure 2A and Supplementary Table S2). The substrate affinities, also for the reverse reaction, all remained in the typical range of those determined for other NAD–MDH isoforms (Supplementary Table S3).

Effect of preincubation with oxidants and re-reduction on enzyme activity and covalent oligomerization

For a cytosolic enzyme, it is not immediately expected that cysteine residues are reversibly modified by oxidation. However, oxidative modification of cyMDH1 occurs *in vitro* upon the addition of oxidants [24,25]. In these studies, oxidizing conditions result in the dimerization of cyMDH1 through the formation of an intermolecular disulfide bond between two monomers. Both, the covalent dimerization as well as the concomitant loss of activity, was reversed by incubation with the reductant DTT, and even more effectively in the presence of reduced thioredoxin h [24,25]. Since in these studies, only cyMDH1 had been analyzed, we were curious to compare all three isoforms concerning their redox-properties and used cyMDH1 as a control. We found that cyMDH isoforms 1 and 2 are both inactivated and covalently dimerize by oxidation (Figure 2), thus confirming the previous studies about cyMDH1 [24,25]. Most interestingly, however, cyMDH3, maintained its low basal activity upon oxidation with 0.5 mM diamide (Figure 2A). Furthermore, beyond its covalent dimerization, multiple covalently-linked oligomers were formed upon oxidation. Their molecular masses correspond to trimer, tetramer, pentamer, up to multiple subunits being covalently linked to each other by disulfide bridges, all being reversible by re-reduction with DTT (Figure 2B). Upon native PAGE, cyMDH1, and cyMDH2 migrate as dimers whether reduced or oxidized (Supplementary Figure S2). The oxidized forms exhibit a small shift to a somewhat larger size/charge caused by a conformational change. This shift is not apparent when C330 is substituted by serine. In contrast, the cyMDH3 wild-type protein forms higher aggregates upon oxidation which are absent from the cyMDH3 C2S C336S double mutant (Supplementary Figure S2).

Looking at the structural model of cyMDH3 in more detail, it is obvious that the unique cysteine residue at position 2 (C2) possibly represents an additional site for the formation of an intermolecular disulfide bridge between cyMDH3 monomers or even enables covalent oligomerization under oxidizing conditions (Figure 2C). The C2 in cyMDH3 is localized in the N-terminal extension of the protein that shows a random-coiled structure. Even though the C2s of two monomers are 46.5 Å apart of each other in the structural model, the N-terminal regions can be expected to show high flexibility. Mimicking this flexibility via moving the N-terminal extensions of two monomers of cyMDH3 in the structural model shows that the cysteine residues at position 2 are getting as close as 3.5 Å enabling the formation of an intermolecular disulfide bridge (Figure 2C). Therefore, we hypothesize that the presence of C2 in cyMDH3 can lead to the formation of covalently linked dimers and/or oligomers under oxidizing conditions that cannot be found for cyMDH1 and cyMDH2 (Figure 2B). To prove this hypothesis, we further investigated the redox properties of cytosolic MDH isoforms and their corresponding cysteine mutants.

Biochemical Journal (2020) **477** 3673–3693
https://doi.org/10.1042/BCJ20200240

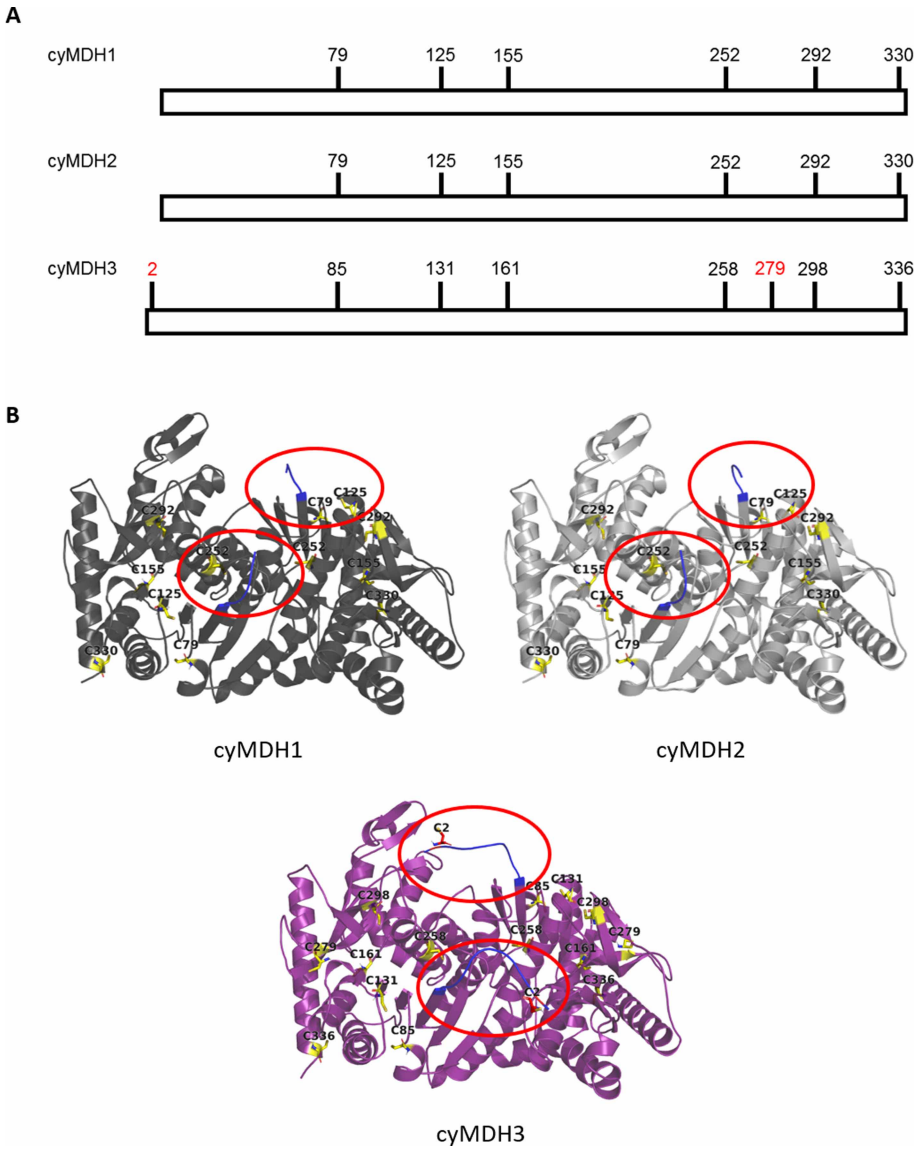

Figure 1. Positions of cysteine residues in cytosolic MDH isoforms from *A. thaliana*.

(**A**) The positions of conserved cysteine residues are shown as black numbers, the two additional cysteine residues of cyMDH3 are indicated in red. (**B**) Structural models of dimeric cyMDH molecules. Structures are shown for cyMDH1 (generated using pdb: 5nuf, shown in dark grey), cyMDH2 (generated via raptorX and the GalaxyHomomer web server, shown in grey) and cyMDH3 (generated via raptorX and the GalaxyHomomer web server, shown in purple). Cysteine residues are marked in yellow and the N-terminal region is marked in blue.

Characterization of cysteine mutants of cyMDH isoforms

To get a better insight into the role of the various cysteine residues and their involvement in the observed oxidative effects on all three cyMDH isoforms, we generated a series of cysteine mutants where every single cysteine residue was substituted by a serine residue. In previous works, it had been already shown for cyMDH1 [24,25] that the C-terminal cysteine residue C330 is responsible for the formation of a disulfide bridge that gives rise to the covalently linked dimer. We could confirm this phenomenon and found an identical behavior for cyMDH2. Replacement of all other cysteine residues in cyMDH1 and cyMDH2 did not affect covalent dimerization or inactivation in the presence of oxidants (Figs. 3 and 4).

In contrast, cyMDH3 exhibited a different pattern where the substitution of C336 (corresponding to C330 in cyMDH1 and cyMDH2) by serine still allowed for the formation of a covalently linked dimer, but to a much

Biochemical Journal (2020) **477** 3673–3693
https://doi.org/10.1042/BCJ20200240

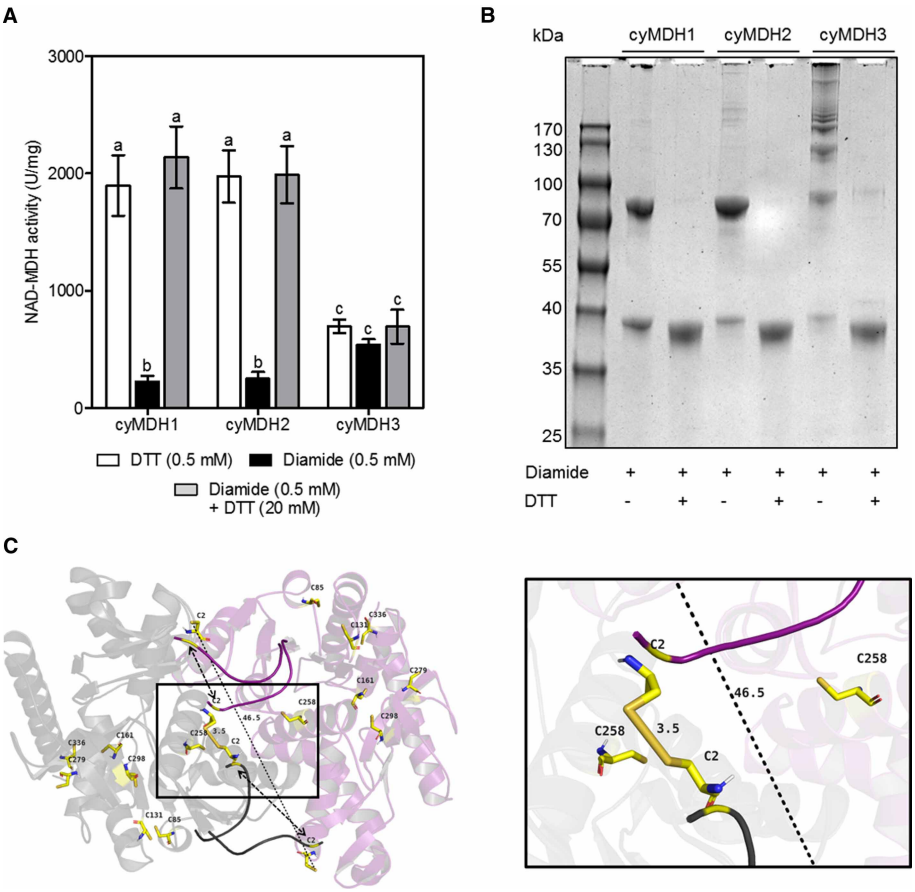

Figure 2. Effect of the redox state on recombinant cyMDH isoforms.

(**A**) Redox-dependent NAD–MDH activity of cyMDHs. The respective enzymes were pre-reduced in 0.5 mM DTT for 30 min and desalted. The enzymes were oxidized with 0.5 mM diamide for 30 min. Reversibility of the oxidation process was shown by adding 20 mM DTT to diamide-treated enzyme. Different letters indicate significant differences of $P \leq 0.01$ that were statistically determined by One-way ANOVA with post-hoc Tukey (HSD) Test ($n = 3$). (**B**) Oligomerization of recombinant cyMDHs. Enzymes were pre-reduced in 0.5 mM DTT for 30 min and desalted. The reduced enzymes were oxidized in the presence of 0.5 mM diamide. Reversibility of the reaction is shown by adding 5 mM DTT to the oxidized enzyme. The pretreated enzymes were separated by non-reducing SDS–PAGE. A representative image of three independent experiments is shown. (**C**) Structural model of cyMDH3. Cysteine residues are marked in yellow. The presence of an additional cysteine residue in the flexible, random-coiled N-terminal region of cyMDH3 (C2) enables the formation of a C2–C2-linked dimer or even higher oligomers.

lesser extent of higher oligomers compared with the wild-type protein and the other single cysteine mutants of cyMDH3. In addition, the substitution of C2 by serine prevents covalent oligomerization, but not covalent dimerization of cyMDH3 (Figure 3). This means that covalently linked cyMDH3 oligomers apparently can only be formed when C2, but not necessarily C336, is present. Only the substitution of both, N-terminal C2 and C-terminal C336, completely prevented the formation of any kind of intermolecular disulfide bridges, and no covalently linked dimers were formed any more in this double-cysteine mutant (Figure 3). Therefore, the presence of C2 and C336 allows for multiple cross-links in the higher molecular mass complexes comprising cross-links within a dimer as well as between monomers of two different dimers and experimentally confirms our herein described hypothesis (see above) that was only based on the structural model of cyMDH3 so far (Figure 2C).

As the activities are concerned, the C330S mutant of cyMDH1 and cyMDH2 lost their sensitivity towards diamide and maintained almost full activity irrespective of reducing or oxidizing preincubation. No major effect of oxidation was detected when cysteine mutants of cyMDH3 were exposed to diamide similar to wild type (Figure 4). However, the substitution of C2 by serine resulted in a strong inhibition upon oxidation, and in an increased activity of reduced cyMDH3 that is similar to the wild type of cyMDH1 and cyMDH2 (Figure 4).

Biochemical Journal (2020) **477** 3673–3693
https://doi.org/10.1042/BCJ20200240

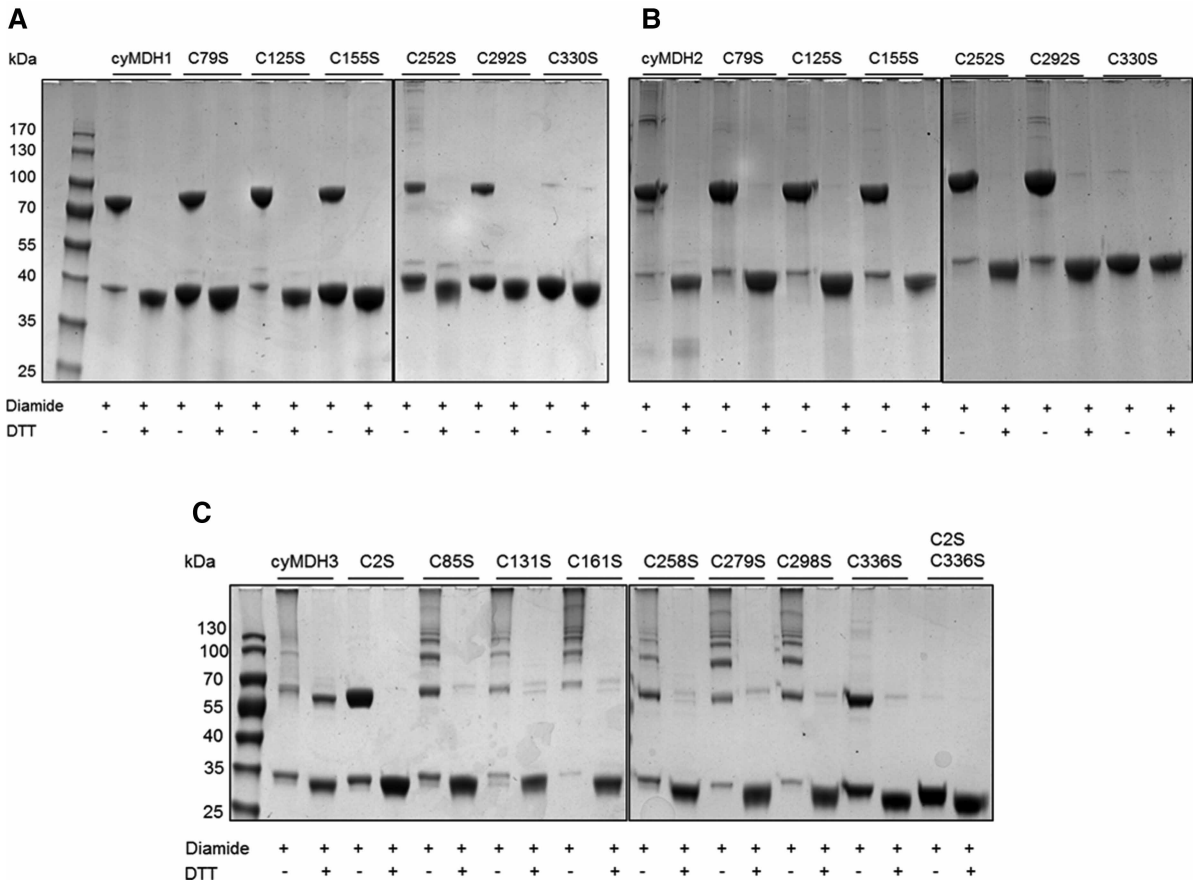

Figure 3. Redox-dependent oligomerization of cyMDH cysteine mutants.

(**A**) cyMDH1, (**B**) cyMDH2, and (**C**) cyMDH3. Enzymes were pre-reduced in 0.5 mM DTT for 30 min and desalted. The reduced enzymes were oxidized in the presence of 0.5 mM diamide. Reversibility of the reaction is shown by adding 5 mM DTT to the oxidized enzyme. The pretreated enzymes were separated by non-reducing SDS–PAGE. The same results were observed in three independent experiments.

Removal of the cysteine on the unique N-terminal sequence extension of cyMDH3 had recovered the properties that are common to cyMDH1 and cyMDH2, namely higher specific activity and redox-dependence.

Structural alignments of cyMDH1, cyMDH2, cyMDH3, and cyMDH3 C2S revealed structural differences close to the N-terminal region of the proteins (Figure 5A). cyMDH1 and cyMDH2 (shown in dark grey and grey, respectively) are characterized by a small α-helical secondary structure while cyMDH3 (shown in purple) is predicted to fold into random-coils in this region. The substitution of C2 by serine in cyMDH3 (shown in blue) leads to the formation of a small α-helix (Figure 5A). Furthermore, the charge distribution around the binding site for NAD^+ of cyMDH1, cyMDH2, cyMDH3, and cyMDH3 C2S differs. While the binding site for NAD^+ is strongly positive in cyMDH1 and cyMDH2, this binding site is less positive or even partially neutral in cyMDH3 (Figure 5B). The substitution of C2 by serine in cyMDH3 also resembles the strongly positive charges surrounding the NAD^+-binding site (Figure 5B). Although the N-terminal region of cyMDH3 is located opposite to the NAD^+-binding site (on the backside), the presence of C2 seems to impose a long-distance effect on this region. However, the differences in charge surrounding the NAD^+-binding site and the presence or absence of a small α-helix in the N-terminal region of cyMDHs could have an impact on the affinity for NAD^+ and might, therefore, result in the observed low activity of the cyMDH3 wild-type protein. This effect would explain why the substitution of C2 by serine results in a similar activity level of cyMDH3 as observed for cyMDH1 and cyMDH2 wild-type proteins under reducing conditions and inactivation upon oxidation.

The double mutant of cyMDH3 lacking both, N- and C-terminal cysteine residues (C2 and C336), however, resembled wild-type cyMDH3 with its low and redox-independent activity. Comparing the effect of the

Biochemical Journal (2020) **477** 3673–3693
https://doi.org/10.1042/BCJ20200240

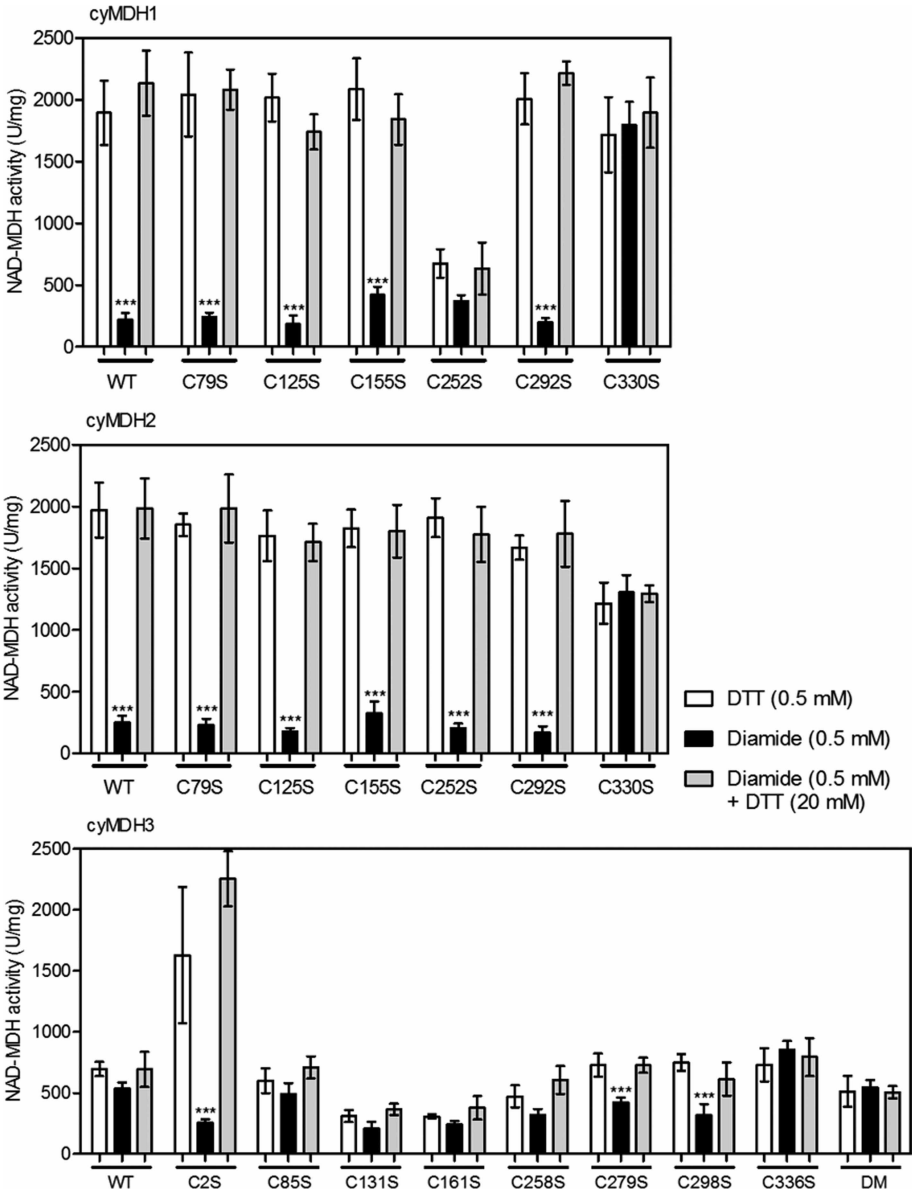

Figure 4. Effect of the redox state on the activity of cysteine mutants of the cyMDH isoforms.

The enzymes were pre-reduced in 0.5 mM DTT for 30 min and desalted. The enzymes were oxidized with 0.5 mM diamide. Reversibility of the oxidation process was checked by adding 20 mM DTT to diamide-treated enzyme. Asterisks indicate significant differences between oxidized and reduced samples of a respective mutant ($P < 0.01$) as determined by One-way ANOVA with post-hoc Tukey (HSD) Test ($n = 3$). (DM: Double mutant C2S & C336S).

C-terminal cysteine residue on covalent dimerization and activity, it is interesting to note that in cyMDH1 and cyMDH2, the lack of the C-terminal cysteine residue abolishes both, covalent dimerization and inactivation by diamide. In contrast, the lack of the C-terminal cysteine residue (C336) in cyMDH3 does not abolish covalent dimerization that in this case is most likely due to the presence of C2 in the N-terminal extension of cyMDH3.

Effect of simultaneous treatment with GSH and diamide on enzymatic properties

Since in the cellular environment, reduced glutathione (GSH) is present at relatively high concentrations in the millimolar range, we repeated the preincubation in the presence of diamide of all three cyMDH isoforms in the

Biochemical Journal (2020) **477** 3673–3693
https://doi.org/10.1042/BCJ20200240

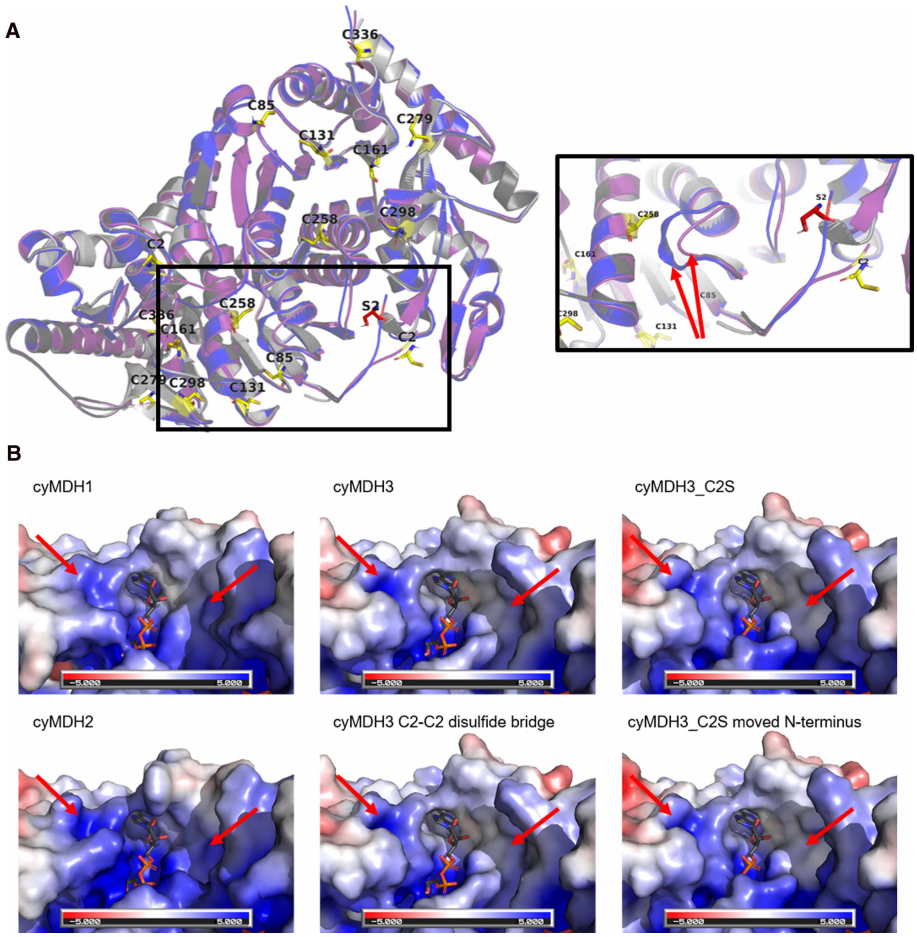

Figure 5. Structural variation at the N-terminal region and the NAD$^+$-binding site of cyMDH isoproteins.
(**A**) Structural alignment of cyMDH1 (shown in dark grey), cyMDH2 (shown in grey), cyMDH3 (shown in purple), and cyMDH3 C2S (shown in blue). Cysteine residues are marked in yellow. The substitution of C2 by serine in cyMDH3 is marked in red. cyMDH3 possesses a random-coil close to the N-terminal region of the protein. In contrast, cyMDH1 and cyMDH2 are characterized by a small α-helical secondary structure. The substitution of C2 by serine in cyMDH3 converts the random coil to a small α-helix as found in cyMDH1 and cyMDH2 wild-type proteins (indicated by red arrows). (**B**) Charge distribution at the surface of the NAD$^+$-binding sites of cyMDHs (red: negative charges; blue: positive charges). The binding site for NAD$^+$ is strongly positive in cyMDH1 and cyMDH2, while this region is less positive or even partially neutral in cyMDH3. Upon substitution of C2 by serine in cyMDH3, the positive charges surrounding the NAD$^+$-binding site re-appear (as indicated by red arrows).

presence of increasing GSH concentrations. Whereas diamide (0.5 mM) alone causes significant inactivation of cyMDH1 and cyMDH2, and no decrease in the basal activity of cyMDH3 (Figure 6), diamide treatment of the enzymes in the presence of 0.5 mM GSH resulted in a completely different pattern. GSH prevents the inactivation of cyMDH1 and cyMDH2 completely. The activity of cyMDH3 was not affected by the oxidative treatment as was the case in the absence of GSH already (Figure 6A). In non-reducing SDS–PAGE, increasing concentrations of GSH prevented covalent dimerization of cyMDH1 and cyMDH2. For cyMDH3, the same treatment resulted in the formation of covalently linked dimers, but not of covalently linked oligomers of higher order as observed in the absence of GSH. GSH at 0.1 mM prevented covalent dimerization of cyMDH1 and cyMDH2, and covalent oligomerization of cyMDH3, respectively, almost entirely (Figure 6B).

To further analyze the role of a specific cysteine residue in covalent dimerization and oligomerization, selected cysteine mutants lacking the C- and N-terminal cysteine residues relevant for forming intermolecular disulfide bridges were subjected to non-reducing SDS gels after oxidation with 0.5 mM diamide in the presence

Biochemical Journal (2020) **477** 3673–3693
https://doi.org/10.1042/BCJ20200240

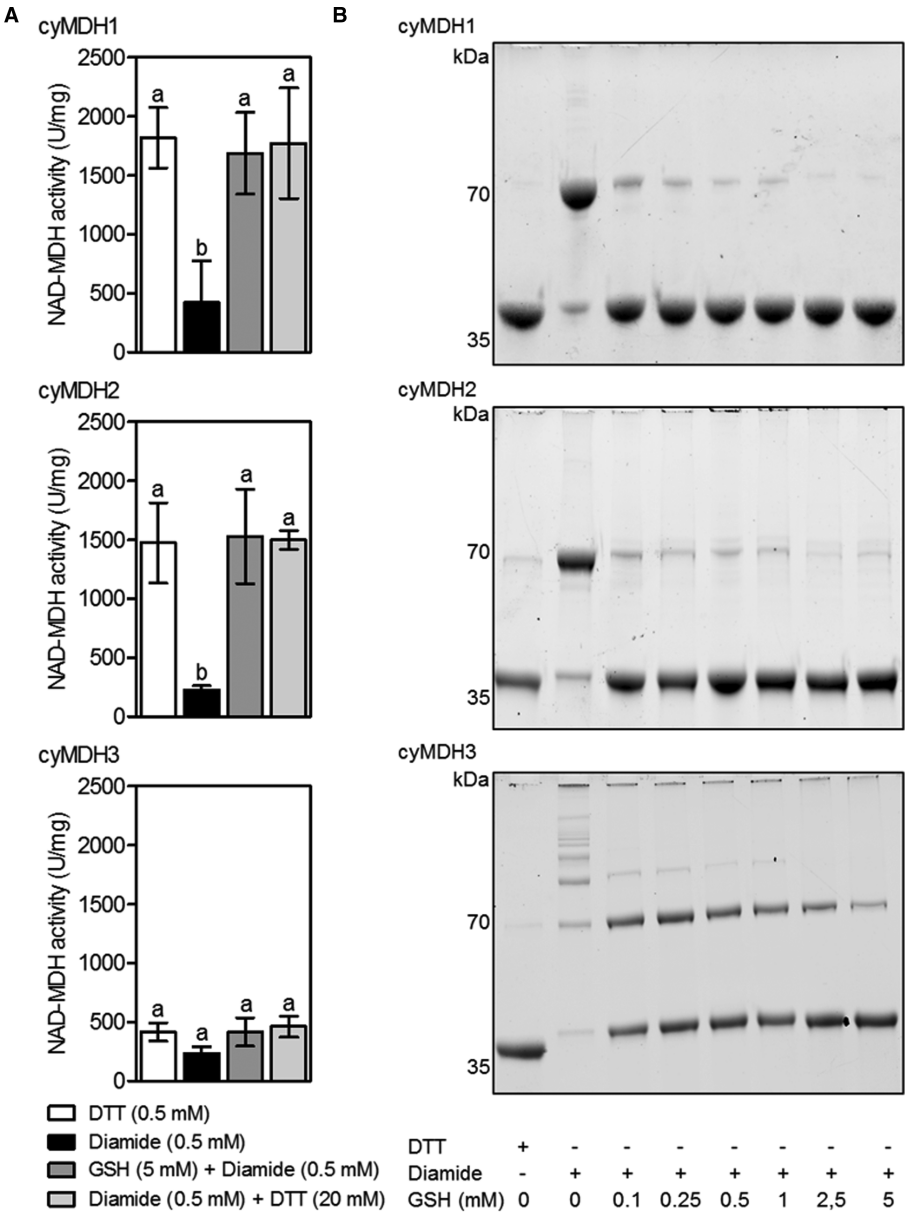

Figure 6. Effect of GSH on the redox state of recombinant cyMDH isoforms.

(**A**) Redox-dependent NAD–MDH activity of cyMDHs. The respective enzymes were pre-reduced in 0.5 mM DTT for 30 min, desalted, and measured. The enzymes were oxidized with 0.5 mM diamide in the presence of 5 mM GSH for 30 min. Reversibility of the oxidation process was shown by adding 20 mM DTT to diamide-treated enzyme. Different letters indicate significant differences of $P \leq 0.01$ that were statistically determined by One-way ANOVA with post-hoc Tukey (HSD) Test ($n = 4$). (**B**) Oligomerization of recombinant cyMDHs. Enzymes were pre-reduced in 0.5 mM DTT for 30 min and desalted. The reduced enzymes were oxidized with 0.5 mM diamide in the presence of the indicated GSH concentration. Reversibility of the reaction is shown by adding 5 mM DTT to the oxidized enzyme. The pretreated enzymes were separated by non-reducing SDS–PAGE. Similar results were observed in three independent experiments.

of increasing GSH concentrations (Figure 7). Even in the presence of a low concentration of GSH (0.1 mM), covalent dimerization of cyMDH1 and cyMDH2 was almost completely prevented (Figs. 6 and 7). A different pattern became apparent for cyMDH3, as covalent dimerization still occurred at GSH concentrations of up to 5 mM. However, low concentrations of GSH prevented the covalent oligomerization of wild-type cyMDH3 and

Biochemical Journal (2020) **477** 3673–3693
https://doi.org/10.1042/BCJ20200240

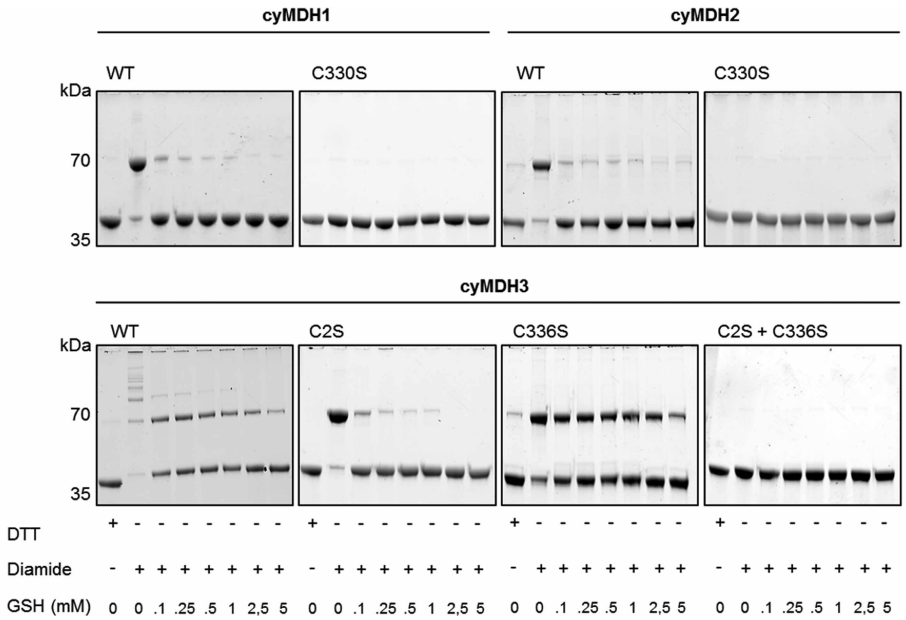

Figure 7. Effect of GSH on the oligomerization of the cysteine mutants of cyMDH isoforms.

Enzymes were pre-reduced with 0.5 mM DTT for 30 min and desalted. The reduced enzymes were oxidized with 0.5 mM diamide in the presence of the indicated GSH concentration. The pretreated enzymes were separated by non-reducing SDS–PAGE. Representative images of three independent experiments are shown.

its C336S mutant, while the C336S mutant of cyMDH3 still covalently dimerized via C2 in the presence of GSH (Figure 7). In contrast, the lack of C2 induced the properties of wild-type cyMDH1 and cyMDH2. The lack of both, C- and N-terminal cysteine residues (C2 and C336), finally, prevented covalent dimerization completely independent of the presence of GSH (Figure 7). The unique role of C2 allowing for covalent dimerization also in the presence of the redox-buffer GSH points to high sensitivity of cyMDH3 for any increase in oxidant as is possible to occur as an early indicator for upcoming cellular redox-imbalances. Covalent dimerization of cyMDH1 and cyMDH2, as well as covalent oligomerization of cyMDH3, would only occur when part of the GSH pool turns oxidized as might be the case under substantial oxidative stress.

Mass-spectrometric determination of cysteine modifications after oxidation in the absence and presence of GSH

To get further insight into cysteine modifications, the oxidized cyMDH isoforms were analyzed by mass spectrometry. The occurrence of cysteine-containing tryptic peptides with masses pointing to carbamylation (free SH-group), S-glutathionylation by the formation of a mixed disulfide with GSH, and intra- or intermolecular disulfide formation is schematically shown in Figure 8. A cross-link between two different monomers at the C-terminal cysteine (C330) was identified for cyMDH1 and cyMDH2 only in the absence of GSH. In the presence of GSH, C330 is predominantly S-glutathionylated and therefore protected from covalent dimerization. The cysteine residues C79 and C252 of both isoforms are also glutathionylated in the presence of GSH (Figure 8). Analyses of cyMDH3 resulted in S-glutathionylation of C2, C85, C161, C258, C279, C298, and C336 (corresponding to C330 in cyMDH1 and cyMDH2) after the oxidative treatment in the presence of GSH. Both, diamide treatment with and without GSH revealed a peptide with two cysteine residues forming an intramolecular disulfide bridge (Figure 8). For cyMDH3, any intermolecular disulfide bridges between monomers leading to covalently linked dimers or oligomers of higher molecular mass as seen in the non-reducing gels (Figs. 2 and 3) could not be detected, probably because not all peptides could be recovered after HPLC separation.

Protection from oxidation by GSH and metabolites

Since *in vivo*, any enzyme is exposed to varying concentrations of its substrates, products, and GSH, we analyzed the redox-properties of the three cyMDH isoforms in the presence of the substrates NAD^+, NADH,

Biochemical Journal (2020) **477** 3673–3693
https://doi.org/10.1042/BCJ20200240

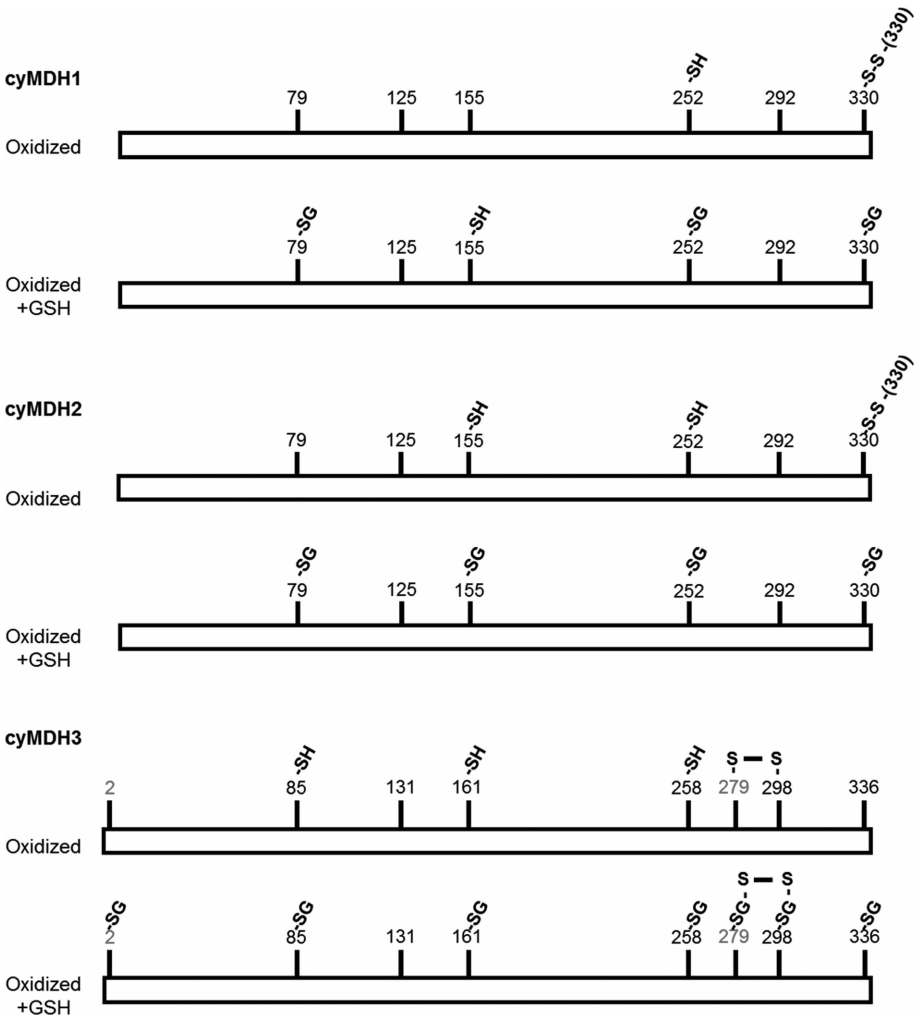

Figure 8. Redox-dependent cysteine modifications of recombinant cyMDH isoforms.

The position of respective cysteine residues is given by black numbers. Enzymes were pre-reduced in the presence of 5 mM DTT for 30 min and desalted. The reduced enzymes were oxidized with 0.5 mM diamide with or without 0.5 mM GSH. Post-translational cysteine modifications (-SH reduced; -S-S- disulfide; -SG S-glutathionylation) were identified by mass spectrometry.

OAA, and malate, as well as with or without GSH. Both covalent oligomerization and activity were measured after preincubation with oxidant in the presence and absence of these small molecules or their combinations. Interestingly, in the absence of GSH, metabolites also served as protecting small molecules that prevented oxidation and covalent dimerization of cyMDH isoforms. Of the tested substrates and products of the MDH reaction, and NADP(H) as a possible indicator for upcoming oxidative stress, only NADH appeared to protect cyMDH1 and cyMDH2 from covalent dimerization, and cyMDH3 from covalent oligomerization while covalent dimerization of this third isoform is still possible (Figure 9A). Protection by NADPH, however, was less efficient compared with NADH. As GSH possesses a similar protective effect as does NADH, we compared both effects and also applied both protecting small molecules simultaneously (Figure 9B). Protection from covalent dimerization by NADH and GSH, whether applied separately or together, was apparent for all wild-type isoforms of cyMDH1 and cyMDH2, and the C2S mutant of cyMDH3. However, both wild-type cyMDH3 and its C336S mutant still covalently dimerized in the presence of NADH and GSH. Apparently, C2 that is present in the N-terminal extension of cyMDH3 appears to be able to undergo C2–C2-linked dimerization even under relatively mild stress since NADH and GSH did not appear to protect and prevent the formation of this particular cross-link.

Biochemical Journal (2020) **477** 3673–3693
https://doi.org/10.1042/BCJ20200240

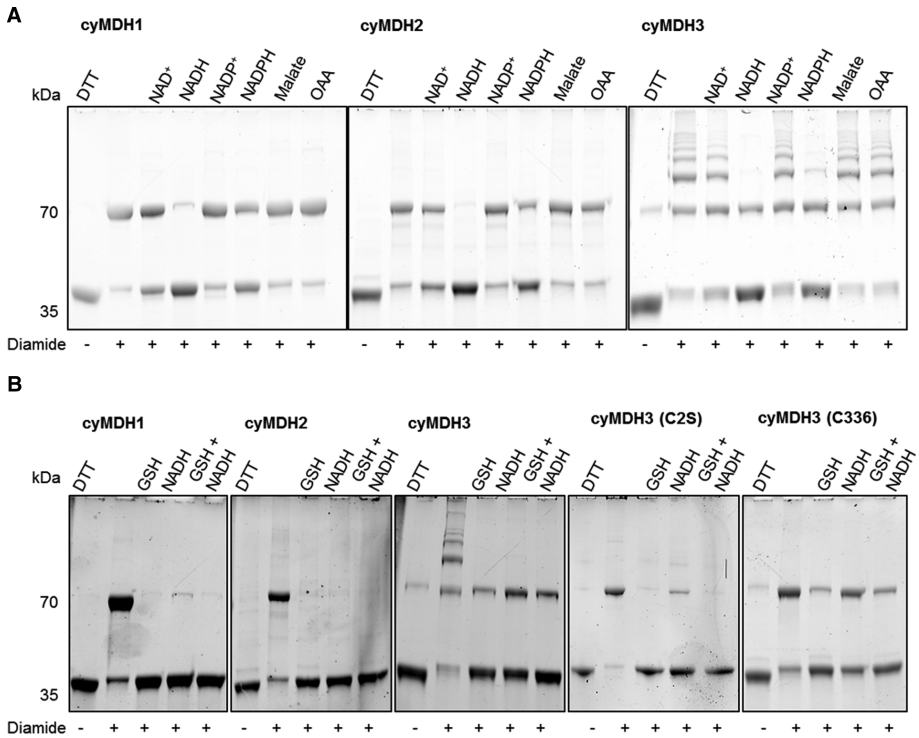

Figure 9. Effect of small molecules on oxidant-induced dimerization and oligomerization of cyMDH isoforms.
Enzymes were pre-reduced in 5 mM DTT for 30 min and desalted. The reduced enzymes were oxidized in the presence of 0.5 mM diamide and (**A**) 5 mM NAD^+, NADH, $NADP^+$, NADPH, malate, or oxaloacetate (OAA), or (**B**) 5 mM GSH, NADH, or both (GSH and NADH), respectively. The pretreated enzymes were separated by non-reducing SDS–PAGE. Similar results were observed in three independent experiments.

Protection from oxidative inactivation was also apparent in the activity responses. Both NADH and GSH separately or together prevented inactivation of cyMDH1 and cyMDH2 by diamide, but no effect was visible for cyMDH3 since its lower activity was unaffected by oxidation already in the absence of protecting agents (Figure 10). NADPH provided partial protection from the inactivation of cyMDH1 and cyMDH2, due to the high similarity with NADH which is, however, more efficient. OAA, malate as well as ATP were ineffective in preventing inactivation (data not shown).

Subcellular localization of cyMDH isoforms in Arabidopsis

To verify the subcellular localization of cyMDH1, cyMDH2, and cyMDH3, GFP-fusion constructs were transiently expressed in isolated mesophyll protoplasts from Arabidopsis. As predicted, strong signals for all three cyMDH isoforms were detected in the cytosol (Figure 11A). Our previous work with cytosolic GAPDH [23,36,37] had shown that oxidative cysteine modifications correlate with its increased occurrence in the nucleus. Therefore, the subcellular localization of all three cyMDH isoforms was analyzed under either reducing (DTT-treated) or oxidizing (diamide-treated) conditions (Figure 11 and Supplementary Figure S3). The nuclear localization of all three isoforms increased significantly after incubation of the protoplasts with 2.5 mM diamide for 2 h but not with DTT (Figure 11).

Interestingly, the co-localization of cyMDH3 with the nuclear marker bZIP was found to be highest under all conditions. In preliminary experiments, H_2O_2, S-nitrosoglutathione (GSNO), and sodium nitroprusside (SNP) did not result in significant stimulation of the nuclear localization of any of the three isoforms (Supplementary Figure S3). The effects of thiol modifications on the enzymatic and structural properties of the cyMDH isoforms, as shown above, might explain the increased nuclear translocation under oxidizing conditions. Having in mind the millimolar concentrations of GSH in the cell, and that cyMDH3 forms covalently linked dimers upon oxidation, even under high GSH concentrations of up to 5 mM, it is conceivable that cyMDH3 might serve as a

Biochemical Journal (2020) **477** 3673–3693
https://doi.org/10.1042/BCJ20200240

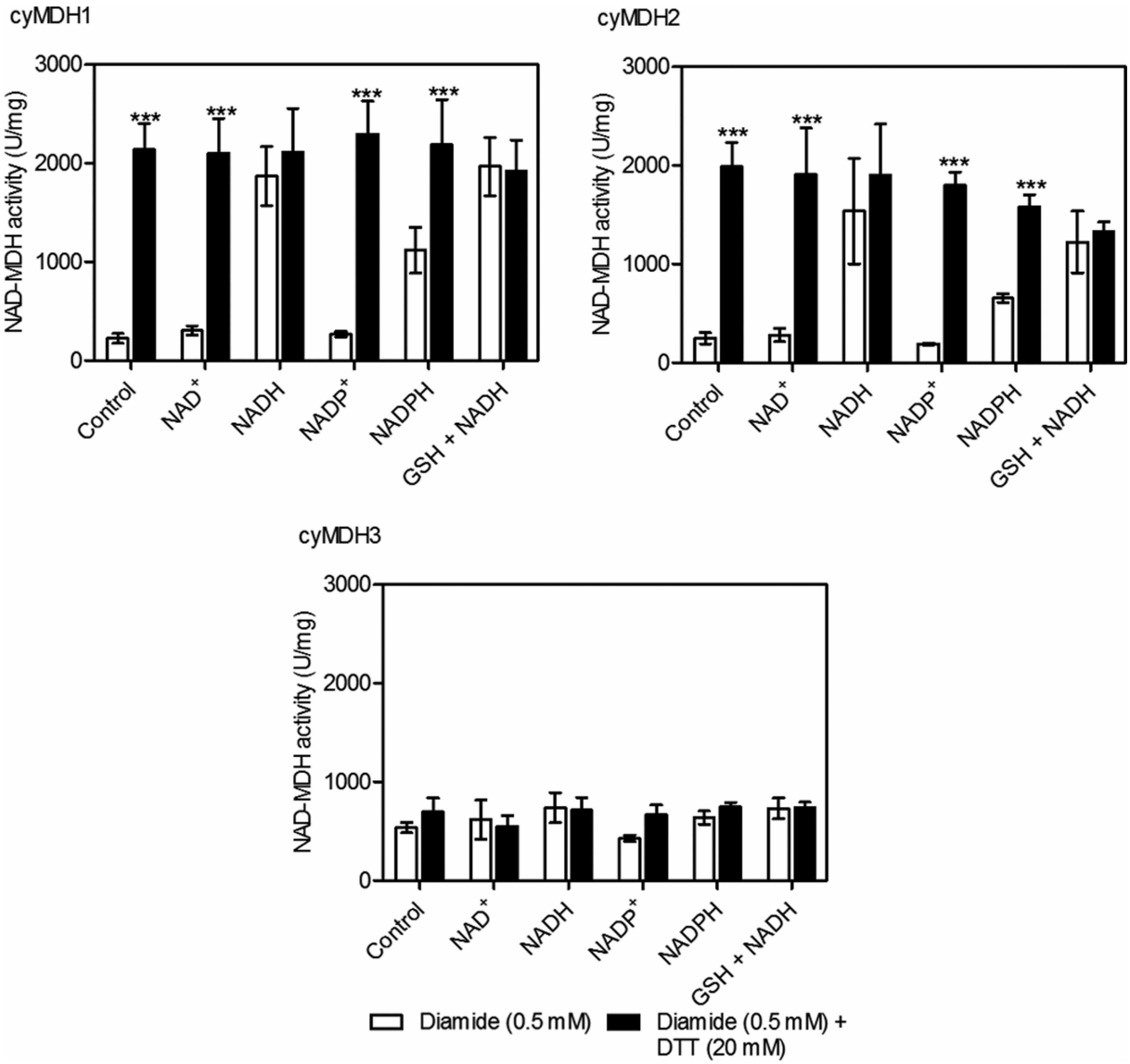

Figure 10. Protection from oxidative inactivation by specific small molecules.

Before measuring the cyNAD-MDH activity, the respective enzymes were pre-reduced in 0.5 mM DTT for 30 min and desalted. The reduced enzymes were oxidized in the presence of 0.5 mM diamide plus 0.5 mM NAD^+, NADH, $NADP^+$, NADPH. The oxidized samples were re-reduced in the presence of 20 mM DTT. Asterisks indicate significant differences between oxidized and re-reduced samples of a respective treatment ($P < 0.01$) as determined by One-way ANOVA with post-hoc Tukey (HSD) Test ($n = 4$).

moonlighting protein in the nucleus (Figs. 6 and 11). The most abundant isoforms cyMDH1 and cyMDH2, however, remain in the non-covalently linked dimeric and therefore active form under these conditions (Figure 6), but also show increased nuclear translocation (Figure 11 and Supplementary Figure S3).

Discussion

The comparative analysis of diamide-induced, oxidative cysteine modifications, in particular, the formation of intermolecular disulfide bridges, reveals differences between the three cytosolic isoforms of NAD-dependent MDH from *A. thaliana*. Oxidation of cyMDH1 and cyMDH2 results in inactivation as previously reported for cyMDH1 [24,25]. In contrast, cyMDH3 is not significantly inactivated under oxidizing conditions.

Biochemical Journal (2020) **477** 3673–3693
https://doi.org/10.1042/BCJ20200240

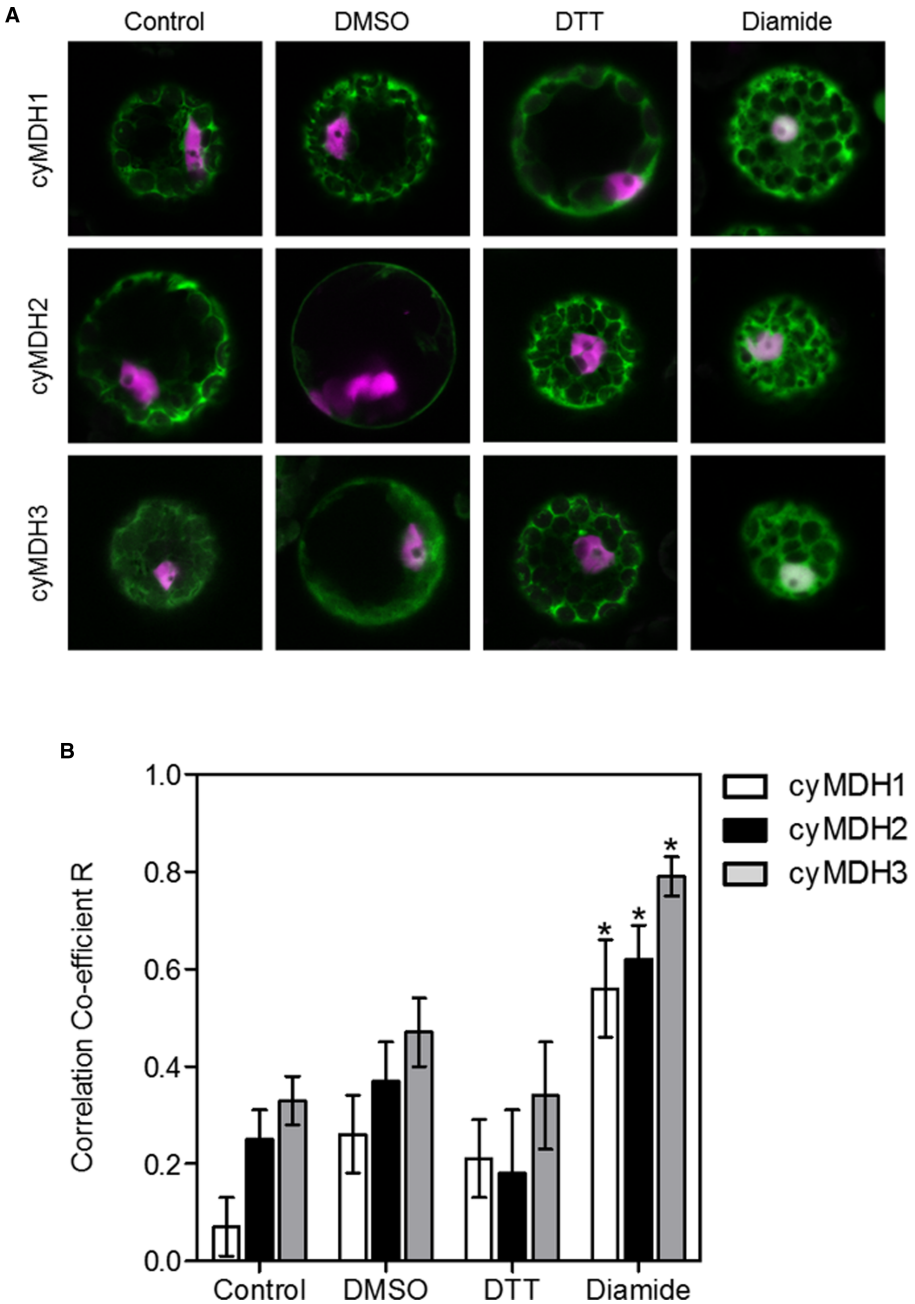

Figure 11. Cytosolic and nuclear localization of cyMDH isoforms.

(**A**) Mesophyll protoplasts were co-transfected with cyMDH isoforms fused to GFP (green) and bZIP-mCherry (magenta) as a nuclear marker as indicated. Co-localization can be seen in false colors as white areas. Representative images are shown for protoplasts treated with DMSO (mock treatment for diamide), DTT, and diamide. (**B**) Correlation of the pattern of bZIP-mCherry and cyMDH isoforms fused to GFP. Images were taken by confocal laser scanning microscopy and analyzed using the co-localization tool of ZEN2011 (Zeiss). Correlation coefficients are given for DMSO, DTT, and diamide. Data are means ± SE from $n \geq 10$ determinations. Asterisks mark data points that were significantly different from the control ($P < 0.01$) as determined by *t*-test.

Simultaneously added GSH, as present in the cellular environment, protects cyMDH1 and cyMDH2 from covalently linked dimerization and inactivation, but cyMDH3 with an N-terminal extension carrying the unique cysteine residue at position 2 (C2) covalently dimerizes independently on the presence of protectants.

In addition to GSH, NADH prevented the covalent dimerization for cyMDH1 and cyMDH2, and the formation of covalently linked higher oligomers for cyMDH3. All cyMDH isoforms were found to undergo nuclear translocation upon addition of diamide to isolated mesophyll protoplasts from Arabidopsis, in particular cyMDH3. As GSH is present at relatively high levels in the cellular environment, diamide treatment of isolated mesophyll protoplasts will lead to S-glutathionylation of cyMDH isoforms thereby preventing covalent oligomerization and at the same time enabling nuclear translocation. These results together with the observed redox-insensitivity and low activity support the conclusion that cyMDH3 functions as a highly sensitive redox-sensor. It will be important in future work to analyze the transcriptional responses induced by cyMDH3 translocated to the nucleus. Since cyMDH1 and cyMDH2 also translocate to the nucleus under oxidizing conditions, all cyMDHs are candidates for integrating redox- and metabolic information and gene expression.

Oxidation of cytosolic enzymes has been found in other cases, e.g. for cytosolic NAD-dependent GAPDH (GapC1 and GapC2 in plants) [23,37]. This glycolytic enzyme provides NADH in conjunction with ATP from the strongly coupled previous step of the 3-phosphoglycerate kinase (3-PGK). Any upcoming oxidative stress would initiate oxidative modifications at specific cysteine residues of GAPDH. Oxidative modification of a catalytic cysteine and a neighboring cysteine residue immediately leads to the inactivation of glycolytic GAPDH, and various moonlighting functions of GAPDH are elicited, among others its nuclear translocation [23]. The glycolytic GAPDH is protected from oxidation as long as the substrate glyceraldehyde-3-phosphate (GAP) is present [37], enabling the integration of the metabolic state and the redox state. Inhibition of glycolysis redirects glucose oxidation to the oxidative pentose phosphate (OPP) pathway generating NADPH for protection from oxidative stress [38]. This example is well-known, although the multiple post-translational modifications, such as S-glutathionylation, S-nitrosylation, or lysine-acetylation that have been found to occur in the plant, yeast, and the animal GAPDH, could not yet be completely connected with its multiple moonlighting functions [39,40].

Various other cytosolic enzymes of central metabolism such as triose-phosphate isomerase [41], isocitrate dehydrogenase [42], and 2-oxo acid dehydrogenase complexes [43] are also subject to redox-regulation and thought to sense redox-imbalances, switching into their moonlighting functions. The here described responses of cyMDHs provide another example for this principle of close control of energy fluxes by a metabolic enzyme functioning as a metabolite-tuned thiol-switch.

In growing tissues, assimilatory processes and central metabolism are of prime importance to increase biomass and to provide energy for cellular functions. Due to compartmentalization, and the fact that membranes are to some extent impermeable for ATP and practically no transporters for reducing equivalents such as NAD(P)(H) exist, distribution of energy equivalents relies on indirect mechanisms using interconvertible metabolites such as triose-phosphate and malate. The latter shuttle system, the so-called malate valve [1,2] consists of dicarboxylate transporters and compartment-specific malate-converting enzymes [44,45]. The chloroplast is equipped with two MDH isoforms. On the one hand, it is equipped with the light-activated NADP–MDH, exporting excess reducing equivalents in the light so that $NADP^+$ remains available as electron acceptor even when NADPH is not consumed inside the chloroplast or to poise the NADPH/ATP ratio. On the other hand, NAD-dependent MDH regenerates NAD^+ for continued plastidial glycolysis that is required for ATP supply by substrate phosphorylation in non-photosynthetic situations. In both cases, malate is exported to the cytosol and can be converted into OAA by cyMDHs. The resulting reducing equivalents (NADH) can either fuel nitrate assimilation in the cytosol and mitochondrial electron transport for ATP synthesis, or be dissipated without ATP synthesis via external NAD(P)H dehydrogenases and alternative oxidases (AOX) if ATP is already in excess. Such final oxidation connected only with thermal dissipation is a versatile means to minimize overreduction or oxidative stress in plants under stressful conditions [46,47].

In the presence of GSH, cyMDH1 and cyMDH2 activities are protected from inactivation upon oxidation by S-glutathionylation at C330. In contrast, cyMDH3 undergoes covalent dimerization via C2–C2 disulfide linkage but no oligomers in the presence of glutathione. The formation of the unique C2–C2 disulfide-linked cyMDH3 then can serve as a redox sensor to induce protective pathways. The protection by NADH, in contrast, is likely based on sterical effects. However, even in the presence of NADH covalent dimerization of cyMDH3 will occur upon oxidation. The here described oxidation of cyMDH1 and cyMDH2 in the absence of GSH and NADH will occur only when the redox-homeostasis of the malate valve and the conversion into NADH are strongly disturbed, and NADH decreases. Due to the inactivation of cyMDH1 and cyMDH2, pathways leading to NADPH generation are required to maintain redox homeostasis. Under these extreme conditions, redirection of malate oxidation would lead to the formation of NADPH and pyruvate (and CO_2) catalyzed by the

Biochemical Journal (2020) 477 3673–3693
https://doi.org/10.1042/BCJ20200240

NADP-dependent malic enzymes (NADP-ME) in the cytosol [44,48]. NADPH is then used for ROS scavenging, and the formed CO_2 can be re-assimilated in the Calvin–Benson cycle. Light-generated ATP and reducing equivalents can then be fed into the assimilation of CO_2, and the risk of overreduction in stressful situations is prevented. The malate shuttle from chloroplasts to mitochondria serves to avoid ROS accumulation and optimization of photosynthesis in Arabidopsis [49] or to induce cell death [50] that are both examples for interorganellar communication, where malate and MDH fulfill prominent functions of energy distribution and ROS protection. In rice, starch grain formation and seed development were found to be negatively affected in the FLO16 mutant lacking a cytosolic MDH [51].

The unique behavior of cyMDH3 enables its function as a sensor that responds very early in cases of upcoming oxidative stress when cellular redox-homeostasis is still maintained and redox-states of GSH (and NADH) are scarcely affected. The main function of this isoform unlikely is linked to its enzyme activity which is low and redox-independent, but rather to its ability for taking over moonlighting functions. Since its C2–C2 disulfide-linked dimer appears already upon minor imbalances, it is a likely candidate for tasks elsewhere in the cell, e.g. as a transcriptional regulator. cyMDH1 and cyMDH2 are protected from inactivation and covalent dimerization by NADH, as well as GSH. The cyMDH3, in contrast, would still form the unique C2–C2-linked dimers as soon as oxidative stress emerges, even when the redox-state of the cytosol is maintained in a reduced state, and GSH (and NADH) redox states are not or little affected. Cellular activities requiring altered transcriptional activities to cope with the upcoming challenge can be induced in a timely and appropriate manner before major imbalance or even damage becomes apparent.

In mammalian cells, cytosolic MDH interacts with p53, a tumor-suppressive transcription factor, in the nucleus and affects transcriptional activity during metabolic stress [52]. This example of MDH as a moonlighting enzyme of central metabolism resembles the well-known situation for GAPDH when metabolism directly regulates transcription and cell fate in general [53,54]. p53, however, is also involved in re-directing metabolic fluxes when glycolysis is turned on in cancer cells and OPP pathway is inactivated, with the GAPDH as a central sensor for imbalances that takes over transcriptional co-activator activity [55–58]. A direct effect of p53 on the expression of malic enzymes, thus down-regulation of NADPH production and induction of senescence, was also shown for mammalian cells [59], providing another example for the dual roles of metabolic enzymes in both energy conversion and signaling activity. Both, in HeLa cells and *A. thaliana*, malate, and, in this case, mitochondrial MDH were shown to be responsible for the induction of programmed cell death [50]. The interaction of mammalian MDH with p53 might indicate an analogy with an interaction of plant MDH with the plant homolog of p53, namely SOG1 (Suppressor Of Gamma Response 1), a transcription factor involved in the stress response upon UV exposure [60], although there is no experimental evidence yet.

Different types and levels of stress are likely to be sensed due to varying, but specific modifications of enzymes involved in energy metabolism. Correlation of the various post-translational modifications and their combinations with specific cellular stress will lead to a more detailed picture of stress responses. Advanced proteomics aiming for the simultaneous analysis of a broad array of covalent modifications needs to be applied with high temporal and spatial resolution after exposure to stress. A first step is the cysteine redoxome as suggested for multiparameter analysis of cellular redox networks with a possible clinical application for the identification of early markers of imbalances [61]. A protein that is subject to multiple cysteine modifications (and additionally lysine acetylation and others) will then function as a built-in sensor and mediator to control energy metabolism and to maintain redox-homeostasis under a broad range of challenging situations. Redox-thiol switches were suggested to fine-tune the central pathways of energy metabolism [62], with S-sulfhydration as another intermediate step during metabolic reprogramming when multiple stress factors need to be integrated [63].

As the cellular redox-state is not only reflected in cysteine modifications, but even more immediate through the redox-couples NAD^+/NADH and $NADP^+$/NADPH, directly connected with the activity of oxidoreductases, both oxidative and reductive stress are sensed at the metabolic level and transferred to a signal-transduction chain [64]. By acting as small molecules affecting protein modifications directly by NAD^+-consuming enzymes [21], or indirectly by their effect upon binding to modification sites on enzymes [7] or on transcription factors [65], these coenzymes can fine-tune energy fluxes as required [5].

Taken together, the cytosol with its metabolic enzymes connects energy fluxes between the various cell compartments and can be seen as a hub for redox-signaling, integrating the different signals and enabling graded and directed responses in stressful situations [66]. In yeast and mammalian cells that consume glucose either for growth and controlled proliferation, stress protection under pathological conditions, or uncontrolled growth

in tumors rerouting of metabolism is under strict control [38,67]. In cancer cells, energy metabolism is reprogrammed to aerobic glycolysis (also known as the Warburg effect) due to defects of the tumor-suppressing transcription factor p53 [68–72], again pointing to connections between energy metabolism and the transcriptional master regulator p53.

In a physiological context, in presence of reduced glutathione, the isoforms cyMDH1 and cyMDH2 are protected from dimerization and inactivation, while cyMDH3 is unique in forming a dimer, but not via the C-terminal cysteine residues. Instead, cross-linkage occurs solely via cysteine C2 which also appears to be responsible for the lower activity of cyMDH3 and its insensitivity towards oxidation. Together with the occurrence of cyMDH3 in the nucleus as observed in isolated mesophyll protoplasts expressing the fluorescent fusion proteins of cyMDH3, these properties might indeed hint to a new function of this minor isoform in transcriptional regulation as its relative occurrence was significantly increased in the nucleus after diamide treatment.

Competing Interests

The authors declare that there are no competing interests associated with the manuscript.

Funding

Financial support was provided by the Collaborative Research Center 944 'Physiology and dynamics of cellular microcompartments' (to A.L. for a lab visit in Osnabrueck), La Trobe University (Research Focus Area (RFA) Grant to J.S.), and the Alexander von Humboldt Foundation (Feodor Lynen Research Fellowship and Feodor Lynen Return Fellowship to J.S.).

Author Contributions

A.L., RSch (Regina Schimpf), K.I.C.Z., A.B., T.S., and S.W. carried out the experiments. J.K. supervised students, participated in discussions, and analyzed the data. A.D. and K.J.D. developed the structural models and discussed results. J.S. and R.S. (Renate Scheibe) conceived the study, participated in its design and coordination, and wrote the manuscript. All authors read and approved the final manuscript.

Acknowledgements

Preliminary experiments have been performed by Nicole Konitzer, Daniela Palgunow, Kira Appel, Katrin Luttmann, Lena Weigel, and Sophia Helmig who were all students in the group of Plant Physiology in Osnabrueck.

Abbreviations

3-PGK, 3-phosphoglycerate kinase; AOX, alternative oxidase; cyMDH, cytosolic malate dehydrogenase; GAP, glyceraldehyde-3-phosphate; GAPDH, glyceraldehyde 3-phosphate dehydrogenase; GSH, reduced glutathione; GSNO, S-nitroso glutathione; NADP-ME, NADP-dependent malic enzyme; OAA, oxaloacetate; OPP, oxidative pentose phosphate; ROS, reactive oxygen species; SNP, sodium nitroprusside.

References

1 Scheibe, R. (2004) Malate valves to balance cellular energy supply. *Physiol. Plant* **120**, 21–26 https://doi.org/10.1111/j.0031-9317.2004.0222.x
2 Selinski, J. and Scheibe, R. (2019) Malate valves: old shuttles with new perspectives. *Plant Biol.* **21**, 21–30 https://doi.org/10.1111/plb.12869
3 Miginiac Maslow, M., Johansson, K., Ruelland, E., Issakidis-Bourguet, E., Schepens, I., Goyer, A. et al. (2000) Light-activation of NADP-malate dehydrogenase: a highly controlled process for an optimized function. *Physiol. Plant* **110**, 322–329 https://doi.org/10.1111/j.1399-3054.2000.1100306.x
4 Scheibe, R. (1981) Thioredoxin m in pea chloroplasts: concentration and redox state under light and dark conditions. *FEBS Lett.* **133**, 301–304 https://doi.org/10.1016/0014-5793(81)80529-7
5 Knuesting, J. and Scheibe, R. (2018) Small molecules govern thiol redox switches. *Trends Plant Sci.* **23**, 769–782 https://doi.org/10.1016/j.tplants.2018.06.007
6 Scheibe, R. (1991) Redox-modulation of chloroplast enzymes: a common principle for individual control. *Plant Physiol.* **96**, 1–3 https://doi.org/10.1104/pp.96.1.1
7 Scheibe, R. and Jacquot, J.P. (1983) NADP-regulates the light activation of NADP-dependent malate dehydrogenase. *Planta* **157**, 548–553 https://doi.org/10.1007/BF00396887
8 Cardaci, S. and Ciriolo, M.R. (2012) TCA cycle defects and cancer: when metabolism tunes redox state. *Int. J. Cell Biol.* **2012**, 161837 https://doi.org/10.1155/2012/161837
9 Kim, S.Y. (2018) Cancer energy metabolism: shutting power off cancer factory. *Biomol. Ther.* **26**, 39–44 https://doi.org/10.4062/biomolther.2017.184

10 Gaude, E., Schmidt, C., Gammage, P.A., Dugourd, A., Blacker, T., Chew, S.P. et al. (2018) NADH shuttling couples cytosolic reductive carboxylation of glutamine with glycolysis in cells with mitochondrial dysfunction. *Mol. Cell* **69**, 581–593 e587 https://doi.org/10.1016/j.molcel.2018.01.034
11 New, M., Van Acker, T., Sakamaki, J.I., Jiang, M., Saunders, R.E., Long, J. et al. (2019) MDH1 and MPP7 regulate autophagy in pancreatic ductal adenocarcinoma. *Cancer Res.* **79**, 1884–1898 https://doi.org/10.1158/0008-5472.CAN-18-2553
12 Wang, Y.P., Zhou, W., Wang, J., Huang, X., Zuo, Y., Wang, T.S. et al. (2016) Arginine methylation of MDH1 by CARM1 inhibits glutamine metabolism and suppresses pancreatic cancer. *Mol. Cell* **64**, 673–687 https://doi.org/10.1016/j.molcel.2016.09.028
13 Hanse, E.A., Ruan, C., Kachman, M., Wang, D., Lowman, X.H. and Kelekar, A. (2017) Cytosolic malate dehydrogenase activity helps support glycolysis in actively proliferating cells and cancer. *Oncogene* **36**, 3915–3924 https://doi.org/10.1038/onc.2017.36
14 Lima Queiroz, A., Zhang, B., Comstock, D.E., Hao, Y., Eriksson, M., Hydbring, P. et al. (2018) miR-126-5p targets malate dehydrogenase 1 in non-small cell lung carcinomas. *Biochem. Biophys. Res. Commun.* **499**, 314–320 https://doi.org/10.1016/j.bbrc.2018.03.154
15 Zhang, B., Tornmalm, J., Widengren, J., Vakifahmetoglu-Norberg, H. and Norberg, E. (2017) Characterization of the role of the malate dehydrogenases to lung tumor cell survival. *J. Cancer* **8**, 2088–2096 https://doi.org/10.7150/jca.19373
16 Lo, A.S., Liew, C.T., Ngai, S.M., Tsui, S.K., Fung, K.P., Lee, C.Y. et al. (2005) Developmental regulation and cellular distribution of human cytosolic malate dehydrogenase (MDH1). *J. Cell. Biochem.* **94**, 763–773 https://doi.org/10.1002/jcb.20343
17 Oh, S.J., Gu, D.R., Jin, S.H., Park, K.H. and Lee, S.H. (2016) Cytosolic malate dehydrogenase regulates RANKL-mediated osteoclastogenesis via AMPK/c-Fos/NFATc1 signaling. *Biochem. Biophys. Res. Commun.* **475**, 125–132 https://doi.org/10.1016/j.bbrc.2016.05.055
18 Lee, S.M., Dho, S.H., Ju, S.K., Maeng, J.S., Kim, J.Y. and Kwon, K.S. (2012) Cytosolic malate dehydrogenase regulates senescence in human fibroblasts. *Biogerontology* **13**, 525–536 https://doi.org/10.1007/s10522-012-9397-0
19 Boukouris, A.E., Zervopoulos, S.D. and Michelakis, E.D. (2016) Metabolic enzymes moonlighting in the nucleus: metabolic regulation of gene transcription. *Trends Biochem. Sci.* **41**, 712–730 https://doi.org/10.1016/j.tibs.2016.05.013
20 Khan, Z., Nisar, M.A., Muzammil, S., Zafar, S., Zerr, I. and Rehman, A. (2019) Cadmium induces GAPDH- and- MDH mediated delayed cell aging and dysfunction in *Candida tropicalis* 3Aer. *Environ. Monit. Assess.* **191**, 490 https://doi.org/10.1007/s10661-019-7631-9
21 Xiao, W., Wang, R.S., Handy, D.E. and Loscalzo, J. (2018) NAD(h) and NADP(H) redox couples and cellular energy metabolism. *Antioxid. Redox Signal.* **28**, 251–272 https://doi.org/10.1089/ars.2017.7216
22 Hildebrandt, T., Knuesting, J., Berndt, C., Morgan, B. and Scheibe, R. (2015) Cytosolic thiol switches regulating basic cellular functions: GAPDH as an information hub? *Biol. Chem.* **396**, 523–537 https://doi.org/10.1515/hsz-2014-0295
23 Schneider, M., Knuesting, J., Birkholz, O., Heinisch, J.J. and Scheibe, R. (2018) Cytosolic GAPDH as a redox-dependent regulator of energy metabolism. *BMC Plant Biol.* **18**, 184 https://doi.org/10.1186/s12870-018-1390-6
24 Hara, S., Motohashi, K., Arisaka, F., Romano, P.G., Hosoya-Matsuda, N., Kikuchi, N. et al. (2006) Thioredoxin-h1 reduces and reactivates the oxidized cytosolic malate dehydrogenase dimer in higher plants. *J. Biol. Chem.* **281**, 32065–32071 https://doi.org/10.1074/jbc.M605784200
25 Huang, J., Niazi, A.K., Young, D., Rosado, L.A., Vertommen, D., Bodra, N. et al. (2018) Self-protection of cytosolic malate dehydrogenase against oxidative stress in Arabidopsis. *J. Exp. Bot.* **69**, 3491–3505 https://doi.org/10.1093/jxb/erx396
26 Kost, B., Spielhofer, P. and Chua, N.H. (1998) A GFP-mouse talin fusion protein labels plant actin filaments in vivo and visualizes the actin cytoskeleton in growing pollen tubes. *Plant J.* **16**, 393–401 https://doi.org/10.1046/j.1365-313x.1998.00304.x
27 Seidel, T., Kluge, C., Hanitzsch, M., Ross, J., Sauer, M., Dietz, K.J. et al. (2004) Colocalization and FRET-analysis of subunits c and a of the vacuolar H^+-ATPase in living plant cells. *J. Biotechnol.* **112**, 165–175 https://doi.org/10.1016/j.jbiotec.2004.04.027
28 Kimata, Y. and Hase, T. (1989) Localization of ferredoxin isoproteins in mesophyll and bundle sheath cells in maize leaf. *Plant Physiol.* **89**, 1193–1197 https://doi.org/10.1104/pp.89.4.1193
29 Källberg, M., Wang, H., Wang, S., Peng, J., Wang, Z., Lu, H. et al. (2012) Template-based protein structure modeling using the RaptorX web server. *Nat. Protoc.* **7**, 1511–1522 https://doi.org/10.1038/nprot.2012.085
30 Baek, M., Park, T., Heo, L., Park, C. and Seok, C. (2017) Galaxyhomomer: a web server for protein homo-oligomer structure prediction from a monomer sequence or structure. *Nucleic Acids Res.* **45**, W320–W324 https://doi.org/10.1093/nar/gkx246
31 Schrödinger, L.L.C. (2015) The PyMOL Molecular Graphics System, Version 1.8
32 Baker, N.A., Sept, D., Joseph, S., Holst, M.J. and McCammon, J.A. (2001) Electrostatics of nanosystems: application to microtubules and the ribosome. *Proc. Natl Acad. Sci. U.S.A.* **98**, 10037–10041 https://doi.org/10.1073/pnas.181342398
33 Dolinsky, T.J., Czodrowski, P., Li, H., Nielsen, J.E., Jensen, J.H., Klebe, G. et al. (2007) PDB2PQR: expanding and upgrading automated preparation of biomolecular structures for molecular simulations. *Nucleic Acids Res.* **35**, W522–W525 https://doi.org/10.1093/nar/gkm276
34 Dolinsky, T.J., Nielsen, J.E., McCammon, J.A. and Baker, N.A. (2004) PDB2PQR: an automated pipeline for the setup of Poisson–Boltzmann electrostatics calculations. *Nucleic Acids Res.* **32**, W665–W667 https://doi.org/10.1093/nar/gkh381
35 Ocheretina, O. and Scheibe, R. (1997) Cloning and sequence analysis of cDNAs encoding plant cytosolic malate dehydrogenase. *Gene* **199**, 145–148 https://doi.org/10.1016/s0378-1119(97)00361-2
36 Aroca, A., Schneider, M., Scheibe, R., Gotor, C. and Romero, L.C. (2017) Hydrogen sulfide regulates the cytosolic/nuclear partitioning of glyceraldehyde-3-phosphate dehydrogenase by enhancing its nuclear localization. *Plant Cell Physiol.* **58**, 983–992 https://doi.org/10.1093/pcp/pcx056
37 Holtgrefe, S., Gohlke, J., Starmann, J., Druce, S., Klocke, S., Altmann, B. et al. (2008) Regulation of plant cytosolic glyceraldehyde 3-phosphate dehydrogenase isoforms by thiol modifications. *Physiol. Plant* **133**, 211–228 https://doi.org/10.1111/j.1399-3054.2008.01066.x
38 Ralser, M., Wamelink, M.M., Kowald, A., Gerisch, B., Heeren, G., Struys, E.A. et al. (2007) Dynamic rerouting of the carbohydrate flux is key to counteracting oxidative stress. *J. Biol.* **6**, 10 https://doi.org/10.1186/jbiol61
39 Sirover, M.A. (2011) On the functional diversity of glyceraldehyde-3-phosphate dehydrogenase: biochemical mechanisms and regulatory control. *Biochim. Biophys. Acta* **1810**, 741–751 https://doi.org/10.1016/j.bbagen.2011.05.010
40 Tristan, C., Shahani, N., Sedlak, T.W. and Sawa, A. (2011) The diverse functions of GAPDH: views from different subcellular compartments. *Cell. Signal.* **23**, 317–323 https://doi.org/10.1016/j.cellsig.2010.08.003
41 López-Castillo, L.M., Jiménez-Sandoval, P., Baruch-Torres, N., Trasviña-Arenas, C.H., Díaz-Quezada, C., Lara-González, S. et al. (2016) Structural basis for redox regulation of cytoplasmic and chloroplastic triosephosphate isomerases from *Arabidopsis thaliana*. *Front. Plant Sci.* **7**, 1817 https://doi.org/10.3389/fpls.2016.01817

42 Niazi, A.K., Bariat, L., Riondet, C., Carapito, C., Mhamdi, A., Noctor, G. et al. (2019) Cytosolic isocitrate dehydrogenase from *Arabidopsis thaliana* is regulated by glutathionylation. *Antioxidants* **8**, 16 https://doi.org/10.3390/antiox8010016
43 Bunik, V.I. (2019) Redox-driven signaling: 2-oxo acid dehydrogenase complexes as sensors and transmitters of metabolic imbalance. *Antioxid. Redox Signal.* **30**, 1911–1947 https://doi.org/10.1089/ars.2017.7311
44 Igamberdiev, A.U. and Bykova, N.V. (2018) Role of organic acids in the integration of cellular redox metabolism and mediation of redox signalling in photosynthetic tissues of higher plants. *Free Radic. Biol. Med.* **122**, 74–85 https://doi.org/10.1016/j.freeradbiomed.2018.01.016
45 Shameer, S., Ratcliffe, R.G. and Sweetlove, L.J. (2019) Leaf energy balance requires mitochondrial respiration and export of chloroplast NADPH in the light. *Plant Physiol.* **180**, 1947–1961 https://doi.org/10.1104/pp.19.00624
46 Selinski, J., Hartmann, A., Deckers-Hebestreit, G., Day, D.A., Whelan, J. and Scheibe, R. (2018) Alternative oxidase isoforms are differentially activated by tricarboxylic acid cycle intermediates. *Plant Physiol.* **176**, 1423–1432 https://doi.org/10.1104/pp.17.01331
47 Selinski, J., Scheibe, R., Day, D.A. and Whelan, J. (2018) Alternative oxidase is positive for plant performance. *Trends Plant Sci.* **23**, 588–597 https://doi.org/10.1016/j.tplants.2018.03.012
48 Maurino, V.G., Gerrard Wheeler, M.C., Andreo, C.S. and Drincovich, M.F. (2009) Redundancy is sometimes seen only by the uncritical: does Arabidopsis need six malic enzyme isoforms? *Plant Sci.* **176**, 715–721 https://doi.org/10.1016/j.plantsci.2009.02.012
49 Raghavendra, A.S. and Padmasree, K. (2003) Beneficial interactions of mitochondrial metabolism with photosynthetic carbon assimilation. *Trends Plant Sci* **8**, 546–553 https://doi.org/10.1016/j.tplants.2003.09.015
50 Zhao, Y., Luo, L., Xu, J., Xin, P., Guo, H., Wu, J. et al. (2018) Malate transported from chloroplast to mitochondrion triggers production of ROS and PCD in *Arabidopsis thaliana*. *Cell Res.* **28**, 448–461 https://doi.org/10.1038/s41422-018-0024-8
51 Teng, X., Zhong, M., Zhu, X., Wang, C., Ren, Y., Wang, Y. et al. (2019) FLOURY ENDOSPERM16 encoding a NAD-dependent cytosolic malate dehydrogenase plays an important role in starch synthesis and seed development in rice. *Plant Biotechnol. J.* **17**, 1914–1927 https://doi.org/10.1111/pbi.13108
52 Lee, S.M., Kim, J.H., Cho, E.J. and Youn, H.D. (2009) A nucleocytoplasmic malate dehydrogenase regulates p53 transcriptional activity in response to metabolic stress. *Cell Death Differ.* **16**, 738–748 https://doi.org/10.1038/cdd.2009.5
53 Sen, N., Hara, M.R., Kornberg, M.D., Cascio, M.B., Bae, B.I., Shahani, N. et al. (2008) Nitric oxide-induced nuclear GAPDH activates p300/CBP and mediates apoptosis. *Nat. Cell Biol.* **10**, 866–873 https://doi.org/10.1038/ncb1747
54 Shi, Y. and Shi, Y. (2004) Metabolic enzymes and coenzymes in transcription: a direct link between metabolism and transcription? *Trends Genet.* **20**, 445–452 https://doi.org/10.1016/j.tig.2004.07.004
55 Hara, M.R., Agrawal, N., Kim, S.F., Cascio, M.B., Fujimuro, M., Ozeki, Y. et al. (2005) S-nitrosylated GAPDH initiates apoptotic cell death by nuclear translocation following Siah1 binding. *Nat. Cell Biol.* **7**, 665–674 https://doi.org/10.1038/ncb1268
56 Jiang, P., Du, W., Wang, X., Mancuso, A., Gao, X., Wu, M. et al. (2011) P53 regulates biosynthesis through direct inactivation of glucose-6-phosphate dehydrogenase. *Nat. Cell Biol.* **13**, 310–318 https://doi.org/10.1038/ncb2172
57 Maddocks, O.D. and Vousden, K.H. (2011) Metabolic regulation by p53. *J. Mol. Med. (Berl)* **89**, 237–245 https://doi.org/10.1007/s00109-011-0735-5
58 Vousden, K.H. and Prives, C. (2009) Blinded by the light: the growing complexity of p53. *Cell* **137**, 413–431 https://doi.org/10.1016/j.cell.2009.04.037
59 Jiang, P., Du, W., Mancuso, A., Wellen, K.E. and Yang, X. (2013) Reciprocal regulation of p53 and malic enzymes modulates metabolism and senescence. *Nature* **493**, 689–693 https://doi.org/10.1038/nature11776
60 Yoshiyama, K.O., Kimura, S., Maki, H., Britt, A.B. and Umeda, M. (2014) The role of SOG1, a plant-specific transcriptional regulator, in the DNA damage response. *Plant Signal. Behav.* **9**, e28889 https://doi.org/10.4161/psb.28889
61 Held, J.M. (2019) Redox systems biology: harnessing the sentinels of the cysteine redoxome. *Antioxid. Redox Signal.* **32**, 659–676 https://doi.org/10.1089/ars.2019.7725
62 Gao, X.H., Li, L., Parisien, M., Mcleod, M., Wu, J., Bederman, I. et al. (2019) Discovery of a redox-thiol switch regulating cellular energy metabolism. *bioRxiv 520411* https://doi.org/10.1101/520411
63 Gao, X.H., Krokowski, D., Guan, B.J., Bederman, I., Majumder, M., Parisien, M. et al. (2015) Quantitative H_2S-mediated protein sulfhydration reveals metabolic reprogramming during the integrated stress response. *eLife* **4**, e10067 https://doi.org/10.7554/eLife.10067
64 Xiao, W. and Loscalzo, J. (2019) Metabolic responses to reductive stress. *Antioxid. Redox Signal.* **32**, 1330–1347 https://doi.org/10.1089/ars.2019.7803
65 Fjeld, C.C., Birdsong, W.T. and Goodman, R.H. (2003) Differential binding of NAD^+ and NADH allows the transcriptional corepressor carboxyl-terminal binding protein to serve as a metabolic sensor. *Proc. Natl Acad. Sci. U.S.A.* **100**, 9202–9207 https://doi.org/10.1073/pnas.1633591100
66 Farooq, M.A., Niazi, A.K., Akhtar, J., Saifullah, Farooq, M., Souri, Z. et al. (2019) Acquiring control: the evolution of ROS-induced oxidative stress and redox signaling pathways in plant stress responses. *Plant Physiol. Biochem.* **141**, 353–369 https://doi.org/10.1016/j.plaphy.2019.04.039
67 Icard, P. and Lincet, H. (2012) A global view of the biochemical pathways involved in the regulation of the metabolism of cancer cells. *Biochim. Biophys. Acta* **1826**, 423–433 https://doi.org/10.1016/j.bbcan.2012.07.001
68 Green, D.R. and Kroemer, G. (2009) Cytoplasmic functions of the tumour suppressor p53. *Nature* **458**, 1127–1130 https://doi.org/10.1038/nature07986
69 Kruse, J.P. and Gu, W. (2009) Modes of p53 regulation. *Cell* **137**, 609–622 https://doi.org/10.1016/j.cell.2009.04.050
70 Liberti, M.V. and Locasale, J.W. (2016) The Warburg effect: how does it benefit cancer cells? *Trends Biochem. Sci.* **41**, 211–218 https://doi.org/10.1016/j.tibs.2015.12.001
71 Potter, M., Newport, E. and Morten, K.J. (2016) The Warburg effect: 80 years on. *Biochem. Soc. Trans.* **44**, 1499–1505 https://doi.org/10.1042/BST20160094
72 Ward, P.S. and Thompson, C.B. (2012) Metabolic reprogramming: a cancer hallmark even Warburg did not anticipate. *Cancer Cell* **21**, 297–308 https://doi.org/10.1016/j.ccr.2012.02.014
73 Boyes, D.C., Zayed, A.M., Ascenzi, R., McCaskill, A.J., Hoffman, N.E., Davis, K.R. et al. (2001) Growth stage-based phenotypic analysis of Arabidopsis: a model for high throughput functional genomics in plants. *Plant Cell* **13**, 1499–1510 https://doi.org/10.1105/tpc.010011